CONF-760716--3

PROCESSES OCCURRING IN SHOCK WAVE COMPRESSION OF ROCKS AND MINERALS*

Dennis E. Grady
Sandia Laboratories
Albuquerque, New Mexico 87115

ABSTRACT

Shock wave studies on rocks and minerals have contributed significantly to current understanding of the earth's interior and have the potential of providing further high pressure physical properties such as transport and higher order thermodynamic properties. Because of this potential, it is important to have a detailed understanding of the physical state achieved by shock compression. With recent advances in time-resolved shock wave instrumentation and improved methods for analyzing continuous stress wave information, a clearer picture is emerging of the processes of yielding and phase transformation occurring during the shock compression. The present report will review recent advances in time-resolved shock wave instrumentation which are currently being used in the study of rocks and minerals and describe the analysis techniques which have been developed to relate shock wave profiles to the thermomechanical processes occurring during shock compression. Evidence for complicating features resulting from yielding in silicates and oxides is reviewed and a physical model for phase transformation and deformation in rocks and minerals is discussed. New supporting data on the shock compression and relief properties of periclase and calcite are also presented.

*This work supported by the U.S. Energy Research and Development Administration, ERDA.
CONTRACT NO. AT(29-1)-789

DISCLAIMER

1. INTRODUCTION

Shock wave studies on rocks and minerals have made a substantial contribution to our current understanding of the earth's mantle. With increasing awareness of mantle dynamics and its coupling within the total earth system, it is clear that improved shock wave techniques could continue to provide useful high pressure physical properties. There is, for instance, a need for measurements of temperature, transport properties, and higher order thermodynamic properties of minerals at pressures existing in the earth's mantle.

It is recognized, however, that prior to such studies a clearer understanding of the physical state achieved by the process of shock compression is required. Some recent results have rendered the simplifying assumption of an equilibrium thermodynamic state at Hugoniot pressures questionable. One must ask how a mineral compressed to a given Hugoniot pressure and temperature compares with a mineral at the same state achieved by static compression techniques. Is pressure and temperature equilibrium achieved in the brief microsecond or less during which a high pressure Hugoniot state can be maintained? Is the material single crystalline or polycrystalline? Are petrographic features peculiar to the shock compression process introduced? Shock compression is a uniaxial phenomenon. Can the compression process introduce anisotropy into an initially isotropic material? Observations by Tynnyaer et al. (1972) of electrical conductivities parallel and perpendicular to the shock front in sodium cloride differing by several orders of magnitude are particularly unsettling in this respect. Can careful preparation of the initial material assist in achieving equilibrium in a shock compression experiment? For instance, would samples composed of sub-micron mineral powder be better than monocrystals?

These and other questions concerning the physical state of the shock compressed material are extremely difficult to access due to its very transient existence. In practice, the nature of the Hugoniot state must be inferred, indirectly, from experimental observations made during and after the shock compression process. Experiments which have been conducted include magnetic, electric, and optical observations during shock compression; flash x-ray studies at Hugoniot pressures; studies of the details of shock and release wave propagation; examination of material recovered from shock wave studies; and others. Such diverse studies place rigid constraints on models describing the thermomechanical processes occurring during shock compression and will eventually lead to a clearer understanding of the states achieved at Hugoniot pressures.

The present paper is focused primarily on the use of shock compression and release wave studies in assessing the material response of rocks and minerals. In recent years, large strides have been made in the development of instrumentation capable of accurately measuring wave profile during shock compression and release. Evolution of the measured wave profiles relate directly to the thermomechanical models governing material response during shock compression. Considerably more complexity has been observed in high pressure wave propagation than was originally envisioned. Complex elastic-plastic response is observed, stress relaxation and attenuation indicative of strain rate effects occur, and details in both compression and release waves due to phase transitions kinetics appear.

In the first section, the experimental methods for measuring time-resolved large amplitude wave profiles which have been, or are becoming, fairly widely accepted are reviewed and contrasted. In the second section, methods which

have been developed to analyze more complex wave propagation experiments will be discussed. In the third section, evidence for complicating features resulting from dynamic yielding in silicates and oxides will be reviewed and a physical model for processes of phase transformation and deformation occurring during shock compression will be discussed. New supporting data on the shock compression and relief properties of periclase and calcite are also presented.

2. CONTINUOUS SHOCK WAVE MEASUREMENTS

A large portion of Hugoniot data available on rocks and minerals was obtained with discrete experimental techniques such as electrical discharge pins (Minshall, 1955) and argon flash gaps (Walsh and Christian, 1955). These methods, although quite reliable, provided only the final shock velocity-particle velocity state and, in some cases, similar information on the elastic precursor wave. These methods depended on the fundamental assumption of a stable Hugoniot state to interpret the high pressure thermodynamic properties.

Increased interest in total large amplitude loading and relief wave behavior both for improved understanding of the deformation process and for additional information regarding high pressure properties has served as impetus for development of continuous recording techniques. Of the various methods which have been explored, some have received fairly wide acceptance and are currently used in a number of shock wave laboratories.

Several of these methods concerned exclusively with the measurement of free surface response include the inclined mirror (Duvall and Fowles, 1962) or inclined prism technique (Eden and Wright, 1965), the inclined wire (Barker et al., 1964), and the capacitor technique (Rice, 1961; Ivanov and Novikov, 1963). These methods will not be discussed here. Several methods which have been developed to measure in-material or quasi-in-material wave profile structures are the piezoelectric, piezoresistant, electromagnetic, and laser interferometry techniques. Since these techniques are currently being used to investigate the shock compression phenomenon in rocks and minerals, it is important to understand the relative strengths and weaknesses of each method including frequency response limitations, stress limitations,

calibration accuracies, and impedance matching difficulties. The objective of this section is to review these techniques and to contrast the various features of each method. Further discussion of these techniques are given by Keeler and Royce (1971), Fowles (1972), and Graham and Asay (1976).

Piezoelectric Techniques

A number of materials have been investigated for shock wave transducers because of their piezoelectric property, including quartz (Graham et al., 1965) and lithium niobate (Graham and Jacobson, 1973). The quartz gauge has become widely used and the present discussion will focus on this material. The piezoelectric properties of quartz and its transducer capabilities have been extensively studied over the past decade (Graham et al., 1965, Ingram and Graham, 1970) and it is presently one of the most accurately calibrated shock wave instruments available.

The quartz gauge consists of a disc of x-cut single crystal quartz with large diameter-to-thickness ratio to insure one-dimensional strain in the active gauge region during transit of the stress wave. The gauge is mounted on the back surface of the sample under test such that the stress wave in the sample enters the gauge and propagates along the x-axis as illustrated in Fig. 1. The transducer has vapor-deposited electrodes and accurate use requires a guard ring electrode (Graham et al., 1965) which assures that measurements are made in a region where one-dimensional strain and electric field persists.

Current is monitored by measuring the voltage drop across a resistive shunt. In a linear approximation, the current produced during shock transit by the piezoelectric effect in the quartz is given by

$$i(t) \cong kA \frac{c_\ell}{d} \sigma(t) \qquad (1)$$

where A is the area of the inner electrode, c_ℓ the wave speed in quartz, d the gauge thickness, σ the stress at the sample-gauge interface, and k is the stress-current coefficient for quartz. Equation (1) is valid for times less than one transit across the gauge thickness.

The quartz gauge has an upper stress limitation of 4.0 GPa (Graham, 1975). X-cut quartz has a Hugoniot elastic limit of 6.0 GPa (Graham, 1974), but shock-induced conductivity limits the upper stress for accurate gauge response. The stress level which can be accurately detected in the sample can be higher than 4.0 GPa if the mechanical impedance of the sample is higher than that of the quartz. Al_2O_3 (corundum) is an example of a mineral with a significantly higher shock impedance.

Time resolution of the quartz gauge system in reproducing the stress profile is quite good being limited only by the rise time of the recording instrumentation and by tilt (nonplanarity) of the stress wave sweeping over the finite active area (typically 4 to 12 mm diameter) of the transducer.

Impedance differences between the quartz and sample material introduce difficulties in interpretation since the measured wave differs from the original wave propagating in the sample material, although it usually retains the essential features of the wave profile. Approximate techniques have been developed for determining the undisturbed profile from the measured profile.

In Fig. 2, a stress wave profile obtained with a quartz gauge on [100] oriented MgO (periclase) is shown (Grady, 1970) which illustrates the measurement capability of this technique. It is of interest to note the character of the initial loading precursor and subsequent stress relaxation which is

significantly more complex than simple elastic-plastic response would predict. The measured elastic precursor amplitude is about 1.9 GPa which corresponds to about 3.1 GPa in the periclase due to the significant impedance difference between the two materials. The finite slope in the late time part of the deformation wave is due to finite strain in the quartz and must be accounted for in the data analysis.

Piezoresistivity Techniques

A number of materials are known to exhibit a stress-induced resistance change, however, only two, ytterbium and manganin, have received serious attention as stress wave transducer materials. The former undergoes a phase transition at about 4.0 GPa restricting its use to stress levels below this value. The latter seems ideally suited for stress wave measurements in rocks and minerals. The manganin gauge has been used routinely at stress levels to 50 GPa (Grady et al., 1974; Murri et al., 1975) and more recently stress wave measurements in granite in excess of 100 GPa have been made (DeCarli, 1975).

Early studies on manganin as a shock wave transducer were conducted by Fuller and Price (1964) and by Bernstein and Keough (1964). Manganin, an alloy with a nominal composition of 84% Cu, 12% Mn, and 4% Ni, exhibits a positive pressure coefficient of resistance and an extremely small temperature coefficient of resistance. Keough et al. (1964) have shown that the pressure coefficient of resistance is independent of temperature between 25 and 500°C for pressures to at least 15 GPa. These properties are particularly favorable for stress wave transducer applications.

Although manganin wire has been used, present methods favor gauge grid patterns photoetched from 25 to 50 μ manganin foil. The grids are usually mounted between slabs of the test sample with the grid face-oriented normal

to the direction of wave propagation as is illustrated in Fig. 3. Also currently used is a four lead gauge configuration, two for application of a constant excitation current and two for measuring the voltage signal induced when the stress wave passes through the sensitive gauge element. Since the current is maintained constant, the transducer provides a voltage-time history which is directly related to the stress-time history through the transducer stress-resistance calibration curve.

The calibration of manganin has not received the exhaustive treatment of the quartz transducer and is complicated by sensitivity to the medium surrounding the element. Bridgeman (1950) reported a linear resistance with static pressure up to 3.0 GPa. Shock loading stress-resistance data to 40 GPa (Lyle et al., 1969; Keough and Wong, 1970) appears to be best fit to a cubic stress-resistance expression. Satisfactory agreement was observed on a similar manganin by Dremin and Kanel (1972). Keough (1968) observed that the coefficient during unloading differs from that on loading and the transducer can be left with a residual net resistance change upon complete unloading. Recent studies on ytterbium (Ginsberg et al., 1973) and silver (Dick and Styris, 1975) have shown that the loading stress-resistance coefficient can be separated into a part due to an intrinsic piezoresistivity effect and a part due to damage-induced defects introduced during plastic yielding at the transducer material. It was further observed that the damage-induced portion saturates, becoming small at high stress levels. Work by Murri et al. (1975) with gauges in rock indicated saturation for manganin and that above about 20 GPa, the loading and unloading coefficients are essentially the same.

Installation of gauges capable of surviving the 50 to 100 GPa stress environment for the required recording time of several μs requires consider-

able care. In granular rocks, differential motion of grains can cause dimpling of the gauge material and provide erroneous stress profile measurements. Also, the piezoelectric property of some mineral types can cause significant noise problems. It has been found that isolating the gauge from the sample with thin sheets of mica can significantly mitigate both of these effects (Murri et al., 1975).

Gauge planes between test samples thinner than 25 to 50 μm are difficult to achieve, and, since this is a region of mechanical impedance different from the sample, it provides for the most serious signal degrading factor in the manganin gauge technique. This problem has been analyzed by Murri et al. (1975). They find that for a 50 μm gauge plane in a typical rock material, a characteristic rise time of 0.035 μs occurs in a sharp shock loading.

In Fig. 4, a stress wave profile obtained from a 1 Ω manganin gauge grid mounted in MgO is shown (Grady, 1970). Maximum stress achieved in the experiment is approximately 6.5 GPa. Comparison of the initial wave shape with the quartz gauge stress profile shown in Fig. 2 illustrates the profile degradation which can occur due to finite thickness of the gauge plane. This comparison somewhat unfairly represents the manganin gauge, however, in that thin sheets of aluminum foil plus mylar were required on each side of the manganin gauge element to shunt a very strong stress-induced polarization signal which results in an approximately 100 μm gauge plane thickness. The manganin gauge profiles shown in Fig. 5 better illustrate the capability of the technique (Grady et al., 1974). All six profiles were obtained in one experiment to a peak stress of about 25 GPa in a quartz rock. Three gauge planes (< 50 μm thickness) at increasing distance from the impact interface illustrate dispersion of the wave with propagation distance and also indicates reproducibility of the man-

ganin gauge technique. The break in slope of the relief wave has been attributed to the transformation of SiO_2 in octahedral coordination to SiO_2 in tetrehedral coordination upon unloading (Grady et al., 1974).

Electromagnetic Techniques

An electromagnetic transducer based on the principle of a moving conductor in a stationary magnetic field has been used extensively to measure particle velocity in shock-loaded solids (Dremin and Adadurov, 1964; Dremin et al., 1965; Petersen et al., 1970). The method has been extended to the measurement of total wave profiles in rock to stress levels of 40 GPa (Grady et al., 1974; Murri et al., 1975). Some features of the electromagnetic gauge are similar to the manganin stress gauge; namely, it is normally installed in-material (between two slabs of the test sample), it can be used over the same stress range, and it has the same resolution difficulties due to wave degradation from the finite thickness of the gauge plane.

The transducer element is typically photoetched from 25-50 μm copper foil in a U shape as is illustrated in Fig. 6. The gauge is sandwiched between slabs of the test material and oriented so that the signal leads are parallel to the applied magnetic field and the active gauge element of length ℓ is perpendicular to the applied field. Wave propagation is directed perpendicular to both the applied field and the active gauge element. Other workers have used a similar gauge geometry but with the signal lead exiting through the back of the test sample (Altshuler et al., 1967). In either case, the particle velocity history as the stress wave sweeps across the gauge plane is linearly related to the induced voltage $\epsilon(t)$ through the relation

$$u(t) = \epsilon(t)/H\ell \qquad (2)$$

where ℓ is the center-to-center active element length and H is the magnetic field intensity. The magnetic field (typically 500 to 1000 gauss) can be generated with pulsed Helmholtz coils or with permanent magnets.

There are several attractive features about the electromagnetic gauge. No calibration is required; the gauge factor is obtained analytically through Eq. 2 and measurement accuracy reduces to careful orientation of the gauge leads, applied field, shock direction, and accurate measurement of the magnetic intensity and active gauge length. The electromagnetic effect is not as sensitive to dimpling caused by differential grain motion and, since the gauge is a low impedance source, piezoelectric noise effects are small.

In Fig. 7, particle velocity profiles obtained by the electromagnetic technique to peak stresses of approximately 25 GPa in Salem limestone are shown (Murri et al., 1975). Note that stress relief which begins when the incident shock emerges at the material free surface appears in the particle velocity record as a further acceleration of the material. The breaks in the relief wave are due to several phase transitions occurring in the calcite during unloading.

Laser Interferometry Techniques

The most accurate technique which has been developed for measuring the particle velocity resulting from impulsive loading of solids is the laser interferometer. With this technique, either the particle velocity history at the specimen free surface or at an interface between specimen and an optical window material can be measured. Several improvements have followed the inception of the technique. Early instruments measured displacement history and velocity was obtained by differentiation of the records (Barker and Hollenbach, 1965). Later, a velocity interferometer was developed which measured the particle velocity directly (Barker, 1968). Recently, the need for a specular reflecting surface or interface, required in early systems, has been eliminated with the development of a diffuse surface velocity interferometer system (Barker and Hollenbach, 1972). The ability to monitor the motion of diffuse surfaces is a particularly important feature since most geological materials cannot be polished to a spectral finish and even if a mirror can be introduced by artificial means, loss of reflectivity usually results from passage of a strong shock wave.

The laser velocity interferometer (specular or diffusely reflecting) is based on the principle of temporally coherent light interference resulting from the moving reflecting surface. The technique uses a beam of laser light which is reflected from a surface on the test specimen. The beam is then split and one portion is delayed a short time, τ with respect to the other (on the order of a few ns) and then recombined. Recombination of the beams effectively differences the displacement at time t and that at time $t - \tau$ and provides an accurate measure of the velocity averaged over the time τ. Barker and Hollenbach (1970) have derived the following expression for the velocity:

$$v(t - \frac{1}{2}\tau) = \frac{\lambda}{2\tau} F(t) \qquad (3)$$

where λ is the wave length of the laser light and $F(t)$ is the fringe count at time t.

The diffuse surface interferometer operates on the same principle as the specular velocity interferometer with the exception that spatial coherence of the reflected light beam is not required. Interferometry with spatially incoherent light can be accomplished provided that the two legs of the interferometer are nearly the same length. To satisfy this requirement and also achieve a relative delay time τ required for velocity interferometry, fused silica etalons are used in one leg of the light beam. The different index of refraction of the etalons makes the apparent path length of the two legs identical, but produces a net delay time. A schematic of the currently used diffuse surface velocity interferometer system is shown in Fig. 8.

In the study of large amplitude wave propagation in solids, it is less ambiguous to measure the in-material wave properties rather than the free surface motion which is complicated by the reflected wave. This can be accomplished with laser interferometry by using transparent window materials and measuring the particle motion at a diffusely reflecting interface between the specimen and window material. Although reflected wave effects are not totally eliminated, they are significantly reduced by careful selection of the impedance of the window material. Stress-induced index of refraction changes occur when the stress wave enters the window material and this must be corrected for in the velocity interferometer equation (Eq. 3). The corrected equation which has been derived by Barker and Hollenbach (1970) is

$$v(t - \frac{1}{2}\tau) = \frac{\lambda F(t)}{2\tau(1 + \Delta\nu/\nu_o)} \qquad (4)$$

where $\Delta\nu/\nu_o$ is the index of refraction correction. A correction due to doppler shift of the reflected beam and wave length dependence of the index of refraction of the etalon material must also be made (Barker and Schuler, 1974). Three window materials have been calibrated, PMMA (polymethyl methacrylate), fused quartz, and z-cut single crystal sapphire, which provide a good selection of different mechanical impedances (Barker and Hollenbach, 1970). Fused quartz remains transparent to at least 6.5 GPa and sapphire appears to lose transparancy at about 13 GPa (Barker and Hollenbach, 1970). The upper stress limit for PMMA has not yet been ascertained although it has been used successfully by Asay and Hayes (1975) to 11 GPa.

Laser interferometry is the most accurate stress wave instrumentation currently available and has the capability of resolving features in the wave structure which are usually not observed with other methods. For measurement of free surface velocity there is, in principle, no upper stress limitation, although with strong shocks local surface jetting can complicate results. With window materials, the high pressure behavior has not been studied thoroughly although efforts are currently underway in this area.

In Fig. 9, a particle velocity profile obtained with a diffuse surface velocity interferometer on single crystal periclase is shown. The maximum stress achieved in the periclase was approximately 4.8 GPa. This result can be compared with the profile obtained with a quartz gauge (Fig. 2) and with a manganin gauge (Fig. 4). Also shown in the figure is a second laser beam which undergoes total internal reflection at the center of the MgO front surface. At the time of projectile impact at the target center, the laser beam

is diverted from its preimpact optical path and provides a very accurate fiducial for determining the transit time across the test specimen (Nunziato et al., 1974).

3. ANALYSIS METHODS

In early shock wave studies on solids, shock velocity and particle velocity were the most readily measured quantities. They were of little intrinsic interest, however, and the Rankine–Hugoniot relations (Duvall and Fowles, 1963) were used to calculate thermodynamic quantities of the high pressure state; namely, the pressure P, the specific volume V, and the specific internal energy E. Application of these relations assumed that transition from the initial state occurred by a single discontinuous shock wave.

With improved instrumentation, it has become recognized that, in many cases, the shock transition process is continuous, complex, and that application of the Rankine-Hugoniot relations is not reliable. Other methods are needed to analyze continuous wave propagation data and to obtain the stress, volume, and internal energy histories. These quantities are not easily obtained from continuous experimental stress-time or particle velocity-time profiles. However, the problem has prompted a number of studies (Fuller and Price, 1964; Fowles and Williams, 1970; Cowperthwaite and Williams, 1971; Grady, 1973; Herrmann, 1973; Seaman, 1974) which have resulted in methods for calculating constitutive relations among stress, particle velocity, specific volume and specific energy directly from the experimental profiles and the conservation equations of mass, momentum, and energy. These results relate to the thermomechanical processes occurring during shock compression and release and assist in understanding and in establishing models to describe these processes.

Conservation Equations

The conservation laws of mass, momentum, and energy for continuous one-dimensional flow are, respectively,

$$\left(\frac{\partial V}{\partial t}\right)_h - \frac{1}{\rho_o}\left(\frac{\partial u}{\partial h}\right)_t = 0 , \tag{5}$$

$$\left(\frac{\partial u}{\partial t}\right)_h + \frac{1}{\rho_o}\left(\frac{\partial \sigma}{\partial h}\right)_t = 0 , \tag{6}$$

$$\left(\frac{\partial E}{\partial t}\right)_h + \frac{\sigma}{\rho_o}\left(\frac{\partial u}{\partial h}\right)_t = 0 , \tag{7}$$

where V is the specific volume, u the particle velocity, σ the stress in the direction of wave propagation, E the specific internal energy, and ρ_o is the initial density. The independent variables are the time t and the material or Lagrangian position h. These equations are generally valid and no recourse to equilibrium states is implied. The only restriction is in Eq. (7) where heat flow and radiation have been neglected.

In terms of the experimental conditions, which are to measure continuous stress-time or particle velocity-time profiles at discrete material positions, it is convenient to express the conservation equations in the following integrated form,

$$V(h,t) = V(h,t_o) + \frac{1}{\rho_o}\int_{t_o}^{t}\left(\frac{\partial u}{\partial h}\right)_t dt , \tag{8}$$

$$u(h,t) = u(h,t_o) - \frac{1}{\rho_o}\int_{t_o}^{t}\left(\frac{\partial \sigma}{\partial h}\right)_t dt , \tag{9}$$

$$E(h,t) = E(h,t_o) - \frac{1}{\rho_o}\int_{t_o}^{t}\sigma\left(\frac{\partial u}{\partial h}\right)_t dt , \tag{10}$$

where the subscripted variables refer to a reference state usually selected in a region of constant state down stream from the profile data to be evaluated. In each of these integral expressions, the term within the integral sign is evaluated from experimental profile data. For instance, if stress histories at several gauge locations are available, the data are used to estimate $(\partial\sigma/\partial h)_t$ and Eq. (9) can be evaluated. Then, in turn, Eqs. (8) and (10) may be evaluated which provides the total stress, volume, energy, and particle velocity history through the compression or relief wave. If particle velocity profiles are measured, Eq. (9) must be formulated differently.

Frequently, various simplifications in the wave propagation occur which simplify evaluation of the conservation equations. Such simplifications may result from a priori information about the material constitutive response or experimental boundary conditions, or they may be required due to experimental limitations such as the number or accuracy of the gauges used.

Shock Waves

Even with the increased resolution of continuous in-material gauges, discontinuities in the wave profiles are often observed. Elastic shocks can occur and deformation shocks can also form due to positive curvature of the stress-strain response. Rarefaction shocks due to phase transitions are also observed during unloading.

If a discontinuity in h-t space occurs in the first order flow variables, V, u, σ, and E, say along a path $h = \zeta(t)$, then the Rankine-Hugoniot relations apply and can be derived from the continuous conservation integral expressions Eqs. 8, 9 and 10. If the velocity of the discontinuity (the Lagrangian shock velocity) is given by $U = d\zeta/dt$ and if the integrands in Eqs. 8, 9 and 10 are transformed by the differential expression $\partial/\partial h = (d/dt - \partial/\partial t)/U$, then application of the mean value theorem to the resulting integrals and proceeding to the limit results in

$$V_1 = V_2 - \frac{1}{\rho_o U}(u_1 - u_2) , \tag{11}$$

$$u_1 = u_2 + \frac{1}{\rho_o U}(\sigma_1 - \sigma_2) , \tag{12}$$

$$E_1 = E_2 + \frac{\sigma_1 + \sigma_2}{2\,\rho_o U} , \tag{13}$$

where the subscripts 1 and 2 refer to values in front of and behind the discontinuity, respectively. When discontinuous flow is observed, then measurement of any two of the flow variables, say shock velocity and the change in particle velocity, are sufficient to determine the change in the remaining flow variables across the discontinuity.

Steady Waves

The steady wave is a simplification which occurs frequently in the study of large amplitude compression waves. Such a wave propagates unchanged in form and at a fixed velocity into a region of constant state. Steady waves can result from a balancing of viscous stresses, which tend to diffuse the wave profile, and positive curvature of the stress-strain relation which tends to steepen the profile.

In steady waves the flow variables are functions only of the single independent variable $\zeta = t - h/U$ where U is the constant velocity of the wave. With this functional constraint, the integral Eqs. 8, 9 and 10 can be evaluated directly and result again in the Rankine-Hugoniot form,

$$V(t) = V_o - \frac{1}{\rho_o U} (u(t) - u_o) , \tag{14}$$

$$u(t) = u_o + \frac{1}{\rho_o U} (\sigma(t) - \sigma_o) , \tag{15}$$

$$E(t) = E_o + \frac{1}{2 \rho_o U} (\sigma(t) + \sigma_o)(u(t) - u_o) , \tag{16}$$

which apply from the reference state to any point on the wave profile. In σ-V-u space the material path from the reference state to the final state is a chord (Rayleigh line). Gauge records of either stress or particle velocity obtained at two positions are required to experimentally verify steady wave propagation.

Simple Waves

Another common simplification results when the material response can be regarded as rate-independent and propagation is into a region of constant state. For such waves, called simple waves, the theory of characteristics shows that the space and time derivatives are related by the differential expression $dx = c\ dt$ where c is the Lagrangian sound speed and depends on the current state of stress at each point in the wave. The conservation equations 8, 9, and 10 then reduce to the Riemann integral form,

$$V(t) = V_o - \frac{1}{\rho_o} \int_{u_o}^{u(t)} \frac{du}{c} , \tag{17}$$

$$u(t) = u_o + \frac{1}{\rho_o} \int_{\sigma_o}^{\sigma(t)} \frac{d\sigma}{c} , \tag{18}$$

$$E(t) = E_o + \frac{1}{\rho_o} \int_{u_o}^{u(t)} \frac{\sigma\ du}{c} . \tag{19}$$

Consequently, two continuous stress gauges, or particle velocity gauges, can be used to determine $c(\sigma)$, or $c(u)$, and the integrals evaluated to determine $V(t)$, $u(t)$, or $E(t)$. Although two gauges are sufficient to estimate c, three gauges are necessary to verify that the paths of constant stress or particle velocity are straight and that simple wave theory is valid.

Centered Waves

A special case of simple wave propagation occurs when the wave is centered at the impact interface of the target specimen. The relief wave, as well as the loading wave, can be centered since some impactor materials, such as fused silica, can produce unloading shock waves which will introduce discontinuous unloading at the impact interface when a thin flyer plate is used. In h-t space, the characteristics are straight lines focused at the point of origin of the discontinuous imput wave, and there is a one-to-one correspondence between the continuous stress $\sigma(t)$ or particle velocity, $u(t)$ and the Lagrangian sound speed, $c = x/(t - t_o)$. The integral Eqs. 8, 9 and 10 can be evaluated with one gauge record although two are required to verify that the wave propagation is centered.

Unsteady Waves

When none of the foregoing simplifications are justified, experimenters have used the integral Eqs. 8, 9, and 10 directly to interpret wave propagation data. Specifically, consider three stress gauge records equally spaced a distance Δh apart. Since the data are continuous in time and discrete in space, this suggests the following centered finite difference approximation (Herrmann, 1973)

$$\left(\frac{\partial \sigma}{\partial h}\right)_{12} = \frac{\sigma_2(t) - \sigma_1(t)}{\Delta h} - \frac{1}{24}\left(\frac{\partial^3 \sigma}{\partial h^3}\right)_{12} \Delta h^2 + \ldots \qquad (20)$$

where the subscript 12 refers to the midway point between gauges 1 and 2. Ignoring second and higher order terms, Eq. 9 can be evaluated to obtain the particle velocity history at the 12 midway point. An expression similar to Eq. 20 can be used to determine the particle velocity history at the 23 midway point and the approximation,

$$\left(\frac{\partial u}{\partial h}\right) = \frac{u_{23}(t) - u_{12}(t)}{\Delta h} - \frac{1}{24}\left(\frac{\partial^3 u}{\partial x^3}\right)_2 \Delta h^2 + \ldots , \qquad (21)$$

can be truncated to the first term and used to evaluate the specific volume and specific internal energy histories through Eqs. 8 and 10. When particle velocity profiles are used, a different analytic approach must be taken (Seaman, 1974).

When stress relaxation is observed in the data or when severe wave attenuation occurs due to rapid overtaking of the loading wave by the relief wave, it has been observed (Grady, 1972; Grady, 1973; Seaman, 1974) that the integrands in Eqs. 8, 9, and 10 can be expressed to make better use of the experi-

mental data. Namely, the space derivative can be written

$$\frac{\partial}{\partial h} = \frac{1}{c_\zeta}\left(\frac{d}{dt} - \frac{\partial}{\partial t}\right) \tag{22}$$

where d/dt is a directional derivative along a path $h = \zeta(t)$ chosen to make optimum use of the wave profile data and $c_\zeta = \zeta'(t)$. The integral Eqs. 8, 9, and 10 then transform to

$$V(h,t) = V(h,t_o) - \frac{1}{\rho_o}\int_{u_o}^{u} \frac{du}{c_\zeta} + \frac{1}{\rho_o}\int_{t_o}^{t}\left(\frac{du/dt}{c_\zeta}\right) dt \ , \tag{23}$$

$$u(h,t) = u(h,t_o) + \frac{1}{\rho_o}\int_{\sigma_o}^{\sigma} \frac{d\sigma}{c_\zeta} - \frac{1}{\rho_o}\int_{t_o}^{t}\left(\frac{d\sigma/dt}{c_\zeta}\right) dt \ , \tag{24}$$

$$E(h,t) = E(h,t_o) + \frac{1}{\rho_o}\int_{u_o}^{u} \frac{\sigma\, du}{c_\zeta} - \frac{1}{\rho_o}\int_{t_o}^{t}\left(\frac{\sigma\, du/dt}{c_\zeta}\right) dt \ . \tag{25}$$

In practice, the paths should be chosen to connect similar features in the gauge records such as the peaks of elastic precursors, wave maxima, or the initiation of rarefaction shocks. When paths have been selected the experimental profiles are smoothed and incremented in time, the directional derivatives are evaluated similar to Eqs. 20 and 21, and Eqs. 23, 24 and 25 are integrated numerically.

When attenuation is not observed in the wave features, paths of constant stress or constant particle velocity are used and $c_\zeta = c_\sigma$, or c_u, which are the wave velocities at constant stress, or constant particle velocity, first discussed by Fowles and Williams (1970). Under this specialization, the last term in Eqs. 23, 24 and 25 vanishes and they take the form

$$V(t) = V_o - \frac{1}{\rho_o} \int_{u_o}^{u} \frac{du}{cu} \quad , \tag{26}$$

$$u(t) = u_o + \frac{1}{\rho_o} \int_{\sigma_o}^{\sigma} \frac{d\sigma}{c\sigma} \quad , \tag{27}$$

$$E(t) = E_o + \frac{1}{\rho_o} \int_{u_o}^{u} \frac{\sigma \, du}{cu} \quad , \tag{28}$$

which represent a generalization of the Riemann integral expressions, Eqs. 17, 18, and 19. Fowles and Williams (1970) and Cowperthwaite and Williams (1971) have derived a number of relations concerning c_σ and c_u. In particular, they have shown that these velocities are equal for simple and steady wave propagation.

Impedance Mismatch Corrections

In both the quartz gauge and the velocity interferometer techniques, the material down stream from the Lagrangian point at which the wave profile measurement is made differs from the test material. Although care is usually exercised in selecting a backing material with mechanical impedance close to that of the test specimen, the match is never exact and wave reflections occur. The measured profile is then a distorted version of the profile originally propagated in the undisturbed test medium. To analyze these profiles, it is necessary to first account for the impedance mismatch and determine the wave profiles in the undisturbed medium.

A scheme frequently used is based on an incremental impedance matching technique and results in relations similar to linear acoustic theory (Grady, 1976). The method is readily appreciated through consideration of the Riemann invariants,

$$J_+ = u + \int^{\sigma} \frac{d\sigma}{\rho_o c} , \tag{29}$$

$$J_- = u - \int^{\sigma} \frac{d\sigma}{\rho_o c} , \tag{30}$$

defined in the test specimen up stream from the interface at which the wave profile is measured. The Riemann invariants J_+ and J_- are constant on right and left facing characteristic paths, respectively.

The backing material, either crystal quartz or a laser window material such as fused silica, has known material properties. That is, if a velocity profile U(t) is measured then the stress profile P(t) is readily determined from the governing constitutive equation. Since both stress and particle velocity must be continuous, it follows that, at the measurement interface,

$$J_+ = U(t) + \int^{P(t)} \frac{d\sigma}{\rho_o c} , \tag{31}$$

$$J_- = U(t) - \int^{P(t)} \frac{d\sigma}{\rho_o c} . \tag{32}$$

Due to invariance, the value of J_+ on a given characteristic would be the same if no interface were present. However, since reflections would not occur in this case, the value of J_- would be zero. Coupling this with Eqs. 29 and 30 results in the following expression for the corrected (undisturbed) particle velocity profile,

$$u(t) = \frac{1}{2} \left(U(t) + \int^{P(t)} \frac{d\sigma}{\rho_o c} \right) . \tag{33}$$

Application is usually in differential form in which case corrections to the differential particle velocity and stress are, respectively,

$$du = \frac{1}{2} \left(d\,U + \frac{d\,P}{\rho_o c} \right) , \tag{34}$$

$$d\sigma = \frac{1}{2} \left(d\,P + \rho_o c\, d\,U \right) . \tag{35}$$

Neglected in this analysis is the slight refraction of J_+ characteristics when they enter the interaction region due to wave reflections, which causes slight arrival time errors upon reaching the measurement interface. These time errors are small, however, if propagation time in the region of interaction is maintained small compared to propagation time in the noninteraction region and if the impedance mismatch is kept small so that bending of characteristics is minimized.

In applying Eq. 34 or 35, the value of c is approximated from the measured Lagrangian wave velocity corresponding to a given stress or particle velocity

level in the wave profile. Since the value of c should correspond to the corrected stress or particle velocity profile, one or two iterations in application of Eq. 34 or 35 can improve the results.

This method of analysis is strictly applicable to rate independent material response. Although frequently used on wave profiles occurring in rate dependent material, it is not clear how representative the corrected profiles are.

Factors Affecting Accuracy

There are a number of error sources in this type of wave form analysis which makes the total accuracy difficult to access. The analysis itself is subject to approximation errors due to truncated terms in the estimation of spacial derivatives. Also smoothing and digitizing the profile records and the process of numerical interpolation, differentiation, and integration are possible error sources to which some attention must be given. In addition, there are experimental errors in the gauge records themselves. Discrepancies in gauge calibration and in time correlation between gauges occur. The time resolution problems with imbedded gauges are significant sources of error and if the gauge is backed by a different impedance material, uncertainties arise due to wave reflections.

Analysis on idealized profiles obtained from known solutions (Cowperthwaite and Williams, 1971; Grady, 1973; Seaman, 1974) have shown that, provided derivatives are estimated along properly chosen paths, truncation errors do not provide for a significant loss in accuracy. The major problem in this regard seems to occur when severe attentuation between gauge profiles is encountered. This can be minimized by proper placement of the gauges.

The dominant source of error resides in the gauge records themselves. Time correlation between records is extremely important since the wave velocity appears to the second power in the stress-volume response. Provided similar gauges are used (for instance, multiple manganin gauges), errors due to calibration or frequency response limitations will appear to the same order in the evaluated stress-strain or stress-particle velocity response. Although similar analysis can be completed using combinations of gauges, say stress and particle velocity gauges, this should probably be avoided due to

the different accuracy problems of the gauge types which can lead to excessive error amplification.

However, if proper attention is given to the numerical details and if the accuracy limitations of the gauge type used are understood, analysis of this type can provide a useful tool in evaluating material response from large amplitude wave propagation data. Details of the stress, strain, strain rate and energy history are more transparent than the measured stress-time or particle velocity-time profiles and provide further insight into the thermomechanical process active during dynamic deformation.

4. YIELDING AND PHASE TRANSITIONS IN MINERALS

Certain features in the Hugoniots obtained from shock compression studies on silicate and oxide minerals have avoided a consistent explanation for some time. Notable complicating features are the metastable portion of the silicate Hugoniots in the mixed phase region and the significant reduction in strength observed above the Hugoniot elastic limit in both silicates and oxides. Recent application of newer shock wave techniques, combined with careful interpretation of earlier shock wave and recovery experiments, has resulted in a plausible description of the physical process occurring in the shock compression of minerals. The basic concepts were reached independently by Ananin et al. (1974), Graham (1974), and Grady et al. (1974, 1975). It would be premature to state that the shock compression process in minerals is now understood. It is not clear whether the description spans all minerals of interest, although certain similarities in experimental results suggest that some aspects of the proposed description occur in most minerals.

The process of dynamic yielding when shock stresses in excess of the Hugoniot elastic limit are achieved seems to be the crucial factor in determining the subsequent compressibility. It is not yet clear whether yielding is a brittle process (complete shearing of atomic planes) or a plastic process due to shear activation and multiplication of dislocations in the lattice. The choice is not critical to the present argument. The important hypothesis is that yielding is a heterogeneous process and that large regions remain virtually undamaged during shock loading. This tenet is supported by a considerable body of experimental evidence which will be discussed shortly. Since yielding is localized to shear zones, energy dissipation due to nonconservative forces in the shock process will also be localized to these zones and lead

to large temperature gradients in the shocked material. Energy considerations on the Hugoniot show that temperatures in these shear zones can be sufficient to cause local melting even though average temperature estimates are still well below melting. Due to low thermal conductivity in these minerals, the nonuniform temperature distribution can persist for some time after passage of the shock front.

A process of adiabatic shear and localized melting can account for most of the curious shock compression effects observed in rocks and minerals including metastable Hugoniots, reduction in strength, release wave behavior, and petrographic features identified in samples subjected to strong shock waves.

Experimental Observations in Shock Compression Studies

Reduction in strength above the Hugoniot elastic limit: The behavior of metals during shock compression is readily explained within the framework of elastic-plastic theory. The Hugoniot above the elastic limit is usually observed within experimental error to maintain a constant offset from the hydrostat equal to $4/3\ \tau_Y$ where τ_Y is the resolved shear stress at yield. Exceptions are normally explained by work hardening or strain rate dependence. The situation for the silicates and oxides is less clear. Studies on polycrystalline corundum (Ahrens et al., 1968; Gust and Royce, 1970) indicate that considerable strength is retained above the Hugoniot elastic limit. On the other hand, single crystal periclase (Ahrens, 1966), corundum (Graham and Brooks, 1971), and quartz (Wackerle, 1962; Fowles, 1967; Graham, 1974) show a substantial loss of strength.

It seems reasonable that, at stress levels where significant adiabatic shearing causes softening or melting in localized planes, the bulk viscosity of the material will be sharply reduced accounting for the observed reduction in strength. There are several reasons why the same behavior might not be expected in fine grain polycrystalline material. First, polycrystals normally exhibit lower Hugoniot elastic limits than the equivalent single crystal, dependent, usually, on the amount of porosity in the material. The lower elastic limit would provide for less elastic shear energy available during the yield process. Second, the separation of shear zones, on the order of 5-20 μ suggested by recovery work in single crystal quartz (Ananin et al., 1973), could be significantly reduced due to grain boundary constraints. Borg (1972) noted one or more sets of planar features, presumably post shock signatures of shear zones, localized to quartz grains in material shocked to 15 GPa. The latter

suggests that the deformation energy in polycrystalline material is more uniformly distributed resulting in less energy per shear zone. Hence, at the same stress level, softening, or melting in the polycrystal should be less than in the single crystal, resulting in greater residual strength.

Metastable Hugoniot; Perhaps the most notable experimental feature observed in the minerals which undergo a primary coordination phase transition under shock compression is the metastable Hugoniot in the mixed phase region (McQueen et al., 1967; Ahrens et al., 1969). The α-quartz to stishovite transition is representative. According to equilibrium thermodynamics, this transition should traverse the mixed phase region on the Hugoniot within a few GPa. Instead the transition which initiates in the neighborhood of 10 GPa does not reach completion until shock pressures on the order of 40 to 50 GPa are achieved.

A number of the primary coordination phase transitions which occur during shock compression have also been observed under static conditions (Stishov and Popova, 1961; Ringwood et al., 1967). They are reconstructive, hence thermally-activated, and are observed to proceed very slowly. When shock compression of sufficient intensity to cause local melting and loss of shear strength occurs, the material state in undamaged regions between the planes of melt should differ little from the static experiment with the exception of a slight temperature rise due to near isentropic volume compression. It is unreasonable to expect that the phase transition rate in these regions should differ significantly from the static case. However, in the shear zones, temperatures are easily sufficient to transform material to the high pressure phase or a liquid form of the high pressure phase by a thermally activated nucleation and growth process, even on the sub-microsecond scale of a shock wave experiment.

It seems then, that at a given stress level, transformation will proceed within the shock front only in those regions which are sufficiently hot. Continued transformation in cooler regions will proceed on a considerably longer time scale and give the illusion, within the duration of a shock wave measurement that an equilibrium Hugoniot state has been attained.

Reduced Sound Velocities on the Hugoniot: The velocity of the initial break of the relief wave following a strong shock wave, or the rate at which radial relief waves propagate into a shock compressed specimen, provide values of the longitudinal sound velocity at high pressure. These methods have been used with some success in metals (Al'tshuler et al., 1960). Recent studies on rock forming minerals differ from the results on metals. Grady et al. (1975) have observed initial relief wave velocities very close to the expected bulk sound velocity in quartz and feldspar, and Bless and Ahrens (1976) have observed relief velocities intermediate between the bulk and longitudinal velocities in corundum. These studies provide further evidence for loss of strength during shock compression and further suggest that the loss of strength can persist for some duration after passage of the shock wave.

Ferrimagnetic Effects Under Shock Compression: Shaner and Royce (1968) have observed that yttrium iron garnet remains ferrimagnetic to at least 40 GPa, substantially above the Hugoniot elastic limit of approximately 5 GPa in this material. Continued ferrimagnetism, a physical phenomenon requiring long range crystalline order, further attests to crystalline integrity of a significant portion of the material at large Hugoniot pressures.

The reduction in magnetization observed by Shaner and Royce (1968) was originally explained strictly by magnetoelastic effects. However, if a condition of thermal heterogeneity persisted at the Hugoniot state then hot zones

would be easily in excess of the Neél temperature and provide for reduction of the bulk saturation magnetization. This alternative explanation is consistent with the observed magnetization versus bias field intensity data which indicates an increasingly reduced stress-induced magnetic anisotropy effect with increased stresses above the Hugoniot elastic limit. This would be expected if reduction in material strength is occurring above the Hugoniot elastic limit.

Petrographic features in pre-shocked material: Extensive studies have been conducted on minerals which have been shock-loaded to stress levels in excess of the Hugoniot elastic limit. A large portion of this work has been on specimens recovered from the vicinity of meteorite impact or nuclear explosions (Bunch, 1968; Chao, 1968; Borg, 1972) and neither the stress level nor the duration of the stress pulse is well determined, although the times of stress application are appreciably longer than can be achieved in a laboratory experiment. Some work on samples which have been recovered from laboratory shock wave experiments has been documented where both the stress level and stress duration are fairly accurately known (DeCarli, 1968).

Planar features (shock lamellae) have been identified in recovered samples of shocked minerals (Stoffler, 1972). They have been studied most extensively in quartz. The lamellae are observed in materials shocked between about 10 to 35 GPa and are identified optically as features separating otherwise undamaged minerals and have spacings of between 2 to 20 μm. They occur preferentially on lattice planes of densest packing. Planar features have been catagorized according to differing optical characteristics, however,

it can be assumed that they correspond to shear zones which originate due to yielding during shock compression and differences occur due to differing stress levels and thermal and strain-rate histories.

Ananin et al. (1973) observed that samples of single crystal quartz shock loaded to just above the Hugoniot elastic limit broke into small rectangular blocks of dimensions 100-200 μm perpendicular to the direction of shock propagation and 5-20 μm parallel to the shock direction. The stresses achieved were substantially lower than the stress region in which post shock planar features are observed, however, the results are suggestive of the same non-uniform yield process.

Klein (1965) conducted recovery experiments on single crystal periclase at shock stresses near 8 GPa. Planar features observed in the recovered samples were noted to increase in separation with increasing distance from the explosive-specimen interface suggesting that, as the shock front widened with increased propagation distance, a coarser shear band structure was favored. He also noted that at large distances, an initial [110] direction preference for the features shifted to a [100] preference.

Shock-recovered specimens of quartz and feldspar are also observed to contain regions of amorphous short-range-order phases. Diaplectic glass (Engelhardt et al., 1967) is observed to predominate in the lower shock pressure region (20-40 GPa) and fused glass more characteristic of those quenched from a liquid state predominate at higher pressures. Diaplectic glass differs from ordinary quartz glass in density, index of refraction, and its character of preserving the morphological signature of the parent crystalline state. Diaplectic glass is thought to be the reversion product of a high density short-range-order solid state phase during pressure release (DeCarli and

Milton, 1965). Alternatively it could be the reversion product of the melted high density phase where freezing occurred prior to total pressure release. In such short times, liquid diffusion processes would be insufficient to totally erase the morphology of the previous crystal state. Boganov et al. (1971) have demonstrated the possibility of such instantaneous freezing of quartz. In quartz, traces of the high density polymorph, stishovite have also been identified in recovered specimens of natural and laboratory shocked material (DeCarli and Milton, 1965).

Phase Transition on Release: Ahrens et al. (1968) using liquid reflection techniques and Grady et al. (1974) using manganin gauges have identified the transition from high density to low density state in quartz on pressure released from Hugoniot states in the mixed phase region. The transition, occurring between 8 to 10 GPa, is well-defined but does not exhibit a rarefaction shock, suggesting some rate dependence in the transition process. Similar studies on feldspar do not show a well-defined transition break; rather, relief paths suggest a continuous transition toward the low density phase (Ahrens et al., 1969; Grady and Murri, 1976). This is probably a consequence of the more complex mineral content of the feldspar specimens studied.

Triangular stress wave input pulses have been used to study the behavior of quartz rock in the mixed phase region (Grady et al., 1974). By analyzing the wave profiles, it was determined that, after the initial rapid transformation to a Hugoniot state in the mixed phase region, a continuing transition from low-to-high density proceeded at a considerably slower rate. A possible explanation for this second transformation rate is thermal diffusion from initial hot spots into regions of untransformed material.

Dynamic Yielding

The silicate and oxide minerals are a class of brittle compounds which, under shock loading conditions, exhibited exceptionally high elastic limits. Theoretical studies on the ultimate strength of solids place probable lower limits of 0.03 G (G = shear modulus) as the shear stress at which failure occurs. Although most solids yield at considerably lower stress levels, the silicates and oxides are observed to yield under shock loading at stresses closely approaching the theoretical limit. Notable examples are single crystal corundum and quartz which exhibit maximum shear stress values of 0.056 c_{44} and 0.11 c_{44}, respectively (Graham and Brooks, 1971).

It has been argued that brittle failure (shear fracture) in these materials is unlikely due to the very large isotropic stress component which occurs in a shock wave experiment, and that an energetically more favorable mechanism of dislocation motion and multiplication must occur. The very high observed elastic limits provide no support for this argument, however, and at present there is little experimental base for choosing a ductile mechanism over a brittle mechanism. Perhaps the most suggestive experimental evidence for a ductile yield process in minerals is the strong similarity between stress relaxation occurring in periclase (Figs. 2 and 9), and probably in quartz as suggested by elastic precurser decay (Ahrens and Duvall, 1966), with that observed in LiF. The latter material has been studied extensively under shock loading conditions and strong correlations between precursor characteristics and dislocation dynamics have been observed.

The reduction in shear stress observed in single crystal silicates and oxides above the Hugoniot elastic limit is certainly linked to the yield process. This reduction in shear stress is frequently equated with loss of

strength at the Hugoniot state and carries the implication that subsequent material response would be fluid like. Initial release wave measurements on quartz and feldspar near the expected bulk sound speed seem to support this (Grady et al., 1975). However, measurements of release wave velocities on corundum (Bless and Ahrens, 1976) suggest reduced but not total loss of strength.

Material softening or melting during shock compression is the most reasonable explanation for the initial and persistent loss of strength, except that estimates of bulk temperature rise during shock compression are far below those required to produce the observed effects. This objection is mitigated somewhat if localization of softened or melted regions occur.

A process of heterogeneous yielding leading to localization of shear is reasonable to expect. The processes of slip occurring during yielding are nonconservative and the energy dissipated must lead to local temperature increase. Plastic processes such as dislocation motion and multiplication are enhanced by increased temperatures and can lead to accelerated yielding in local hot regions. Analysis of constitutive relations with temperature dependence, coupled with the thermomechanical equations of motion, show that homogeneous yielding can be subject to Taylor instabilities (Bellman and Pennington, 1955). As an example, Holtzman and Cowan (1961) have used a continuum description of dynamic yielding in solids of the form

$$\tau = \tau_y + \eta \frac{\partial u}{\partial x} \tag{36}$$

where τ is the shear stress, τ_y, the shear stress at yield, η, the dynamic viscosity, and u, the particle velocity normal to the direction x. A reasonable form for temperature dependence of the viscosity is

$$\eta = \eta_o e^{-a(T-T_o)} \quad . \tag{37}$$

Under conditions of flow normal to the x direction due to the shear stress τ, the equation of motion is

$$\frac{\partial u}{\partial t} - \frac{1}{\rho_o} \frac{\partial \tau}{\partial x} = 0 \tag{38}$$

and the energy equation, assuming Fourier heat conduction, is

$$\frac{\partial T}{\partial t} - \chi \frac{\partial^2 T}{\partial x^2} = \frac{1}{\rho_o c} \tau \frac{\partial u}{\partial x} \quad . \tag{39}$$

T, χ, c, and ρ_o are the temperature, thermal diffusivity, specific heat, and density, respectively. A first variation solution to Eqs. 36, 37, 38 and 39 (Grady, 1976) show that the solution is unstable to homogeneous deformation. From the analysis one finds, if τ_y is assumed small, that the wave length of perturbations at maximum growth rate is

$$\lambda_m = \frac{2\pi}{\dot{\gamma}} \left[\frac{\rho_o \chi c^2}{a^2 \eta_o^2} \right]^{\frac{1}{4}} , \tag{40}$$

the maximum growth rate is

$$\alpha_m = \frac{a \eta_o}{\rho_o c} \dot{\gamma}^2 , \tag{41}$$

and the cutoff wave length below which perturbations will not grow is

$$\lambda_c = \frac{2\pi}{b\dot{\gamma}} \left[\frac{\rho_o \chi c}{a a \eta_o} \right]^{\frac{1}{2}} , \tag{42}$$

where $\dot{\gamma}$ is the plastic strain rate.

Expressions for finite τ_y are similar but more complicated. Comparison of the optimum wave length with the periodicity of shear banding observed in shock-loaded aluminum are in reasonable agreement. Material property data are presently insufficient to make similar comparisons in minerals, however, the variations in planar feature separation with propagation distance observed by Klein (1965) appears consistent with this explanation. Taylor instabilities, therefore, seem to provide a plausible explanation for the heterogeneous yield process apparently occurring in these materials.

Some previously unreported experimental results by the author on single crystal periclase, although preliminary, provide some interesting observations on the process of yielding in oxide minerals. In this work, samples of periclase 3.3 mm in thickness were shock-loaded and unloaded in the [100] direction by planar impact of [0001] oriented sapphire plates (3.15 mm thickness) to stress levels between 4.8 and 11.2 GPa. [0001] sapphire response is elastic in this region. Diffuse surface velocity interferometry was used to measure the back interface particle velocity profile between the periclase sample and a sapphire window material. A second laser beam was reflected internally off of the center of the sample impact face. Upon impact the beam is diverted and provides a very accurate time of arrival fiducial as was described in Section 2. In the present experiments, wave transit times within 1% could be measured. The experimental set-up was previously illustrated in Fig. 9.

Profiles obtained in the three experiments conducted are shown in Fig. 10. The initial elastic loading wave consists of a sharp rise to a stress level of about 2.5 GPa followed by significant stress relaxation. The measured precursor velocity of 9.34 ± 0.05 km/s is consistent with ultrasonic velocities measured by Spetzler (1970). Subsequent loading to the Hugoniot state pro-

ceeds in the deformation wave. Note that the width of the deformation wave decreases with increasing peak stress. Two features in the relief wave structure are identified in Fig. 10. The first will be called the initial elastic release, the second, the initial plastic release. The structure of the release wave is similar to elastic-plastic response observed in release waves for certain metals (Asay and Hayes, 1975) and strongly suggests that material strength persists, or has recovered, in periclase at the Hugoniot state.

In Fig. 11, elastic precursor stress-strain points and the final Hugoniot states are identified in the stress-volume plane. Also shown is the periclase hydrostatic compression curve estimated with a Murnaghan equation extrapolation of ultrasonic single crystal data to 0.8 GPa (Spetzler, 1970). Within experimental uncertainty, the Hugoniot stress volume data indicate total collapse to the hydrostat. Shock velocities lower than the local bulk sound speed were measured above the Hugoniot elastic limit which also suggests collapse toward the hydrostat. Reduced shock velocities have also been noted by Graham (1974) in single crystal sapphire and quartz.

Release wave velocities obtained from the shock wave experiments are compared with extrapolation of ultrasonic data (Spetzler, 1970) in Fig. 12. The initial elastic release velocities are similar to those reported by Bless and Ahrens (1976) on corundum. Velocities are below expected [100] longitudinal velocities but are substantially above expected bulk sound velocities. On the other hand, the plastic release velocities are very close to the bulk sound velocity.

In Fig. 11, the initial release paths are shown for the two highest Hugoniot states. The release paths deviate significantly from the hydrostat and imply a shear stress build-up through an axial stress drop of

1.45 ± 0.1 GPa at which point subsequent unloading appears to parallel the hydrostat.

It appears then that single crystal periclase, under shock compression, collapses to the hydrostat and exhibits, perhaps briefly, loss of shear strength. However, subsequent material response during the release wave, which arrives about 0.5 μs after the Hugoniot state is attained, suggests substantial recovery of material strength. The observations in periclase are not inconsistent with a process of local shearing and local heat generation leading to loss of strength during shock compression. Energy dissipated during shock compression in periclase is about a factor of 20 less than occurs in quartz at the same stress level. Calculations show that melted regions could not persist in periclase for the 0.5 μs separating the shock and relief wave due to thermal conduction away from those regions although residual thermal heterogeneity could result in a reduced shear modulus. Hence, recovery of material strength prior to relief wave arrival would seem reasonable. Observations such as these in which the shear strength is time-dependent illustrates the complexity of the compression features of shock-loaded minerals.

The Phase Transformation

Silicates: It is fortunate that the phase transitions in the silicate minerals can proceed within the submicrosecond time scale of a shock wave experiment. If this were not the case, the use of shock waves to investigate physical properties of minerals at pressures existing in the lower mantle would be severely limited. One is justified in asking how these transitions can proceed on such a rapid time scale when the same transitions, under static conditions, are observed to be extremely sluggish.

Considerable effort has been devoted to the study of phase transitions occurring under conditions of shock wave loading and a fairly extensive literature has developed on the theory of shock-induced phase changes and their consequences on the propagation of finite amplitude waves (Duvall and Horie, 1965; Andrews, 1973; Hayes, 1974). In most of these studies equilibrium thermodynamics is assumed and, when rate dependence is considered, it is usually assumed, at least tacitly, that a homogeneous process occurs. The consequences of a heterogeneous yield process on phase transition kinetics have not been considered.

Dremin and Breusov (1968) have argued that a polymorphic transition cannot proceed yielding during shock compression. If yielding proceeds on localized planes by an adiabatic shear process in silicate minerals and if near or total loss of strength has occurred due to near or total melting on these planes, then the regions between planes will experience nearly hydrostatic pressure. It is difficult to see, then, how conditions differ significantly from static compression conditions except for the potentially quite different thermal state. Teller (1962) concluded that shear phenomena at high pressures play an important role in chemical processes. Rather than direct shear activation, however, he suggests that the shear process contributes to dissipative energy accumulation which aids thermal activation in the chemical process. This last idea seems worth pursuing with regard to the completion of reconstructive phase transitions under shock loading conditions. In the next few paragraphs, some consequences of a heterogeneous failure mechanism on the primary coordination transformation in silicate

minerals will be addressed. Attention will be focused on the α-quartz-stishovite transformation for which considerable shock wave data is available. We will make the simplifying assumption that yielding under shock compression is confined to an equidimensional rectangular lattice with lattice dimension d. Assume also that the dissipative energy incurred during shock compression is uniformly distributed on this lattice as thermal energy and that the regions or blocks between planes undergo isentropic compression only. The dissipated energy can be estimated from the measured Hugoniot and isentropic compression properties of the shocked mineral.

We will further assume that the processes of yielding and phase transition are separate in time with yielding proceeding on the shorter time scale as suggested by Dremin and Breusov (1968). This will allow attention to be focused strictly on the phase transition process.

At this point, we will consider one deformation plane located at the Lagrangian coordinate $h = 0$ with the h axis, $h > 0$, normal to the plane. At time $t = 0$ a certain amount of thermal energy, consistent with energy dissipated in the shock process, is deposited at the point $h = 0$. A state of uniform hydrostatic pressure P exists throughout. For $t > 0$ heat will flow from the deformation plane into the adjacent material which is initially at a temperature $T_s(P)$ resulting strictly from isentropic compression.

Assume that heat transfer is governed by Fourier conduction only. Estimates of radiative heat transfer at the calculated temperatures are small within the time scale of interest. A constant specific heat, c, and thermal diffusivity, χ will be used.

A primary coordination phase change is assumed to be thermally-activated with a frequency factor and activation energy independent of the pressure.

A simplified form of the Johnson-Mehl equation (Burke, 1965) will be used to describe the reaction rate of the transition. This description then leads to the equations

$$\frac{\partial T}{\partial t} = \chi \frac{\partial^2 T}{\partial h^2} + \frac{\ell}{c} \frac{\partial \lambda}{\partial t} , \tag{43}$$

$$\frac{\partial \lambda}{\partial t} = F e^{-\frac{A}{kT}} (1 - \lambda) , \tag{44}$$

which govern heat flow and the transition reaction rate in the neighborhood of one deformation plane. λ is the mass fraction of the high density phase, F and A are the frequency factor and activation energy, respectively, and ℓ is the latent heat of transition. Eqs. 43 and 44 are coupled and not readily solvable. If the second term on the right hand side of Eq. 43 is ignored, the heat flow equation can be solved separately. This is justified on two accounts. First, this term is small in the time scale of interest. Second, the dissipative energy at the Hugoniot state, which was estimated in this work by simply subtracting the isentropic elastic energy of quartz from the total Hugoniot energy, already includes the latent heat of transition.

With this simplification, solution of the thermal conduction equation results in the temperature distribution at time t of

$$T = T_s(P) + \frac{Q}{\sqrt{4\pi \chi t}} e^{-h^2/4\chi t} \tag{45}$$

where $Q = \epsilon/\rho_o c$ and ϵ is the thermal energy per unit area initially deposited at h = 0. Some temperature profiles at increasing times are illustrated in the upper half of Fig. 13.

It is a characteristic of thermally-activated reactions, due to the exponential form of the Boltzmann factor, that reactions which proceed very slowly at a given temperature can proceed very rapidly when the temperature is raised a few hundred degrees. If a temperature T_A is considered such that the coordination transformation can proceed within the time scale of a shock compression wave, say $\dot{\lambda} \simeq 10^8/s$. Then the solution, Eq. 45, acts as a thermal wave and carries the temperature T_A to the untransformed material. A path of constant temperature is governed by the differential equation,

$$\frac{dh}{dt} = \frac{h}{t}\left(1 - \frac{x}{h^2/2t}\right) , \tag{46}$$

and is shown in Fig. 13. Note that a given temperature level does not continue to propagate away from h = 0 but reaches a maximum distance,

$$\delta = \sqrt{2\tau\chi} , \tag{47}$$

in a time

$$\tau = \frac{Q^2}{4\pi\,\chi e(T_A - T_s(P))^2} , \tag{48}$$

and then recedes, determining the domain of material which is transformed rapidly by the thermal wave from that which is not.

If a specific energy E_D, due to energy dissipated in the Hugoniot process is distributed uniformly over the deformation plane lattice with lattice parameter d, a value

$$Q = \frac{E_D\, d}{3\, c} \tag{49}$$

is obtained. If transformation proceeds to a maximum distance δ from the

deformation plane and if the lattice parameter is d, the resulting mass fraction of transformed material is

$$\bar{\lambda} = \frac{6\delta}{d} , \tag{50}$$

τ, Q, and δ can be eliminated from Eqs. 47-50 resulting in an expression for the temperature,

$$T_A = T_s(P) + \sqrt{\frac{2}{\pi e}} \frac{E_D}{c\bar{\lambda}} , \tag{51}$$

capable of transforming the material within the shock front at the expressed reaction rate. E_D can be estimated from the quartz Hugoniot as previously described. The fraction of the high density phase $\bar{\lambda}$ in the mixed phase region can also be estimated from the relation of the Hugoniot state to the high and low density phase boundaries. This was accomplished for quartz between P = 15 - 35 GPa. We found T_A to have a constant or slightly increasing value between 1250 - 1350°K. Using a value of $\dot{\lambda} = 10^{-4}/S$ for the quartz-stishovite reaction rate at T = 500°K, then a reasonable value of 50 kcal/mole is estimated for the activation energy. The calculation also suggests that transformation cannot proceed instantaneously but is controlled by propagation of the thermal wave into the untransformed material. Eq. 48 predicts a value of τ = 0.25 μs at a pressure of 25 GPa, although better than 75% of the transformation occurs within less than 0.05 μs. This value is consistent with shock wave rise times which have been observed (Wackerle, 1962; Grady et al., 1974).

Calcite: The mineral calcite is observed to experience two phase transitions below stress levels of 2.0 GPa under both static and shock loading conditions. At these lower stress levels very accurate shock wave measurements

can be made, providing increased understanding of the processes of shock-induced phase changes in rocks and minerals. The calcite I-II and calcite II-III transitions occur statically at stress levels of about 1.45 and 1.75 GPa, respectively (Bridgman, 1939; Singh and Kennedy, 1974). Recent shock wave studies on Solenhofen limestone (Schuler and Grady, 1976) using interferometry techniques have revealed the effect of both transitions in the structure of compression and relief wave propagation. Shock wave profiles obtained on Vermont marble have been particularly distinct in this respect, however, and one such profile is shown in Fig. 14.

In the experiments on Vermont marble samples approximately 8 mm in thickness were impacted with fused silica plates approximately 4.8 mm in thickness. The resulting impact provided a square wave input stress pulse of approximately 1.6 μs duration and a stress amplitude dependent on the impact velocity. Maximum impact stress achieved in the experiment shown in Fig. 14 was 3.5 GPa. Samples were backed with fused silica laser window material and the particle velocity profile which evolved over 8 mm of propagation distance was measured at the marble-fused silica interface. The marble and fused silica have quite similar mechanical impedance characteristics.

In the particle velocity profile shown in Fig. 14, features resulting from different physical mechanisms are quite distinct. The dynamic stress-volume path, also shown in Fig. 14, was determined assuming self similarity of both the compression and release wave. Although self similarity has not yet been strictly verified for marble, wave propagation results obtained in limestone suggest that it is a reasonable approximation. The dynamic stress-volume path is compared with the calcite hydrostat (Singh and Kennedy, 1974). Similar features occurring in the profile and in the stress-volume path are numbered in Fig. 14.

The Hugoniot elastic limit (1 in Fig. 14) was achieved in marble prior to onset of the calcite I-II phase transition (2 in Fig. 14). This differs from observations in limestone where no separation of the plastic and transition waves are observed (Schuler and Grady, 1976). The calcite I-II transition initiates at an axial stress of about 1.2 GPa, somewhat less than the 1.45 GPa transition pressure observed statically in single crystal calcite (Singh and Kennedy, 1974). The shock wave transition stress is consistent, however, with ultrasonic studies on marble where local stress concentrations are believed responsible for the early initiation of the I-II transition. In the loading wave profile, the calcite II-III transition (3 in Fig. 14) is believed to initiate at a stress of about 2.4 GPa, somewhat higher than the observed static value. Note also that the dynamic loading path (representative of the Hugoniot in this material) is significantly higher than the hydrostat similar to the metastable Hugoniots observed in the silicates.

Features in the release wave also mirror characteristics of the calcite phase transitions. Point 4 in Fig. 14 is thought to be initiation of the reverse calcite II-III transition and point 5 the reverse calcite I-II transition. The release wave signatures of each transition differ dramatically.

The calcite I-II transition is known to be displacive (Merrill and Bassett, 1975), a higher order coordination transformation, and, hence can be expected to proceed at a very rapid rate (Buerger, 1972). Formation of a rarefaction shock wave on release due to the calcite I-II transition is consistent, then, with a rapid displacive transformation. This author is not aware of the nature (displacive or reconstructive) of the calcite II-III transition. However, comparison of the release wave shape due to the calcite II-III transition (4 in Fig. 14) with the high pressure release wave shape in quartz (Fig. 5)

due to the reverse α-quartz-stishovite phase transition show considerable similarity in structure. The α-quartz-stishovite transition is a primary coordination transformation with a finite reaction rate. Rate dependence associated with the reverse phase change is expected to provide the profile shape observed in quartz (Fig. 5) or as is indicated from the reverse calcite II-III transition in Fig. 14. We tentatively suggest, therefore, that the calcite II-III transition is reconstructive and that the release wave signature of reconstructive and displacive transformations differ significantly.

Finally, it should be noted that there is no indication of elastic-plastic response in the release wave for marble (providing other features have been correctly identified). Also, comparison of the initial release wave velocity with the calcite III phase static bulk modulus determined by Singh and Kennedy (1974) shows this velocity to be very close to the expected bulk value. This result is consistent with release wave behavior observed in quartz and feldspar (Grady, et al.), both of which undergo a phase transition, but differ from behavior observed in corundum (Bless and Ahrens, 1976) and periclase (present work) which do not experience a phase transformation.

5. CLOSURE

Recent advances in both experimental techniques and methods for analyzing wave profile data have contributed to the study of shock processes in solids. There is at present, a notable lack of time-resolved wave profile data on rocks and minerals approaching mantle pressures. Existing studies, however, have suggested a potential framework for a theory describing the shock processes of yielding and phase transition in silicate and oxide minerals, although further experimental studies are needed to confirm and to quantify some of the mechanisms proposed.

Our present understanding of the shock compression process in minerals is still not adequate to dictate the optimum experimental conditions necessary to prepare a thermodynamic Hugoniot state at pressures and temperatures compatible with mantle conditions. Results obtained to date, however, suggest some possibilities. Perhaps a starting material of gem quality single crystals in shock wave experiments is not the optimum situation. A process of heterogeneous yielding during shock compression and the subsequent non-uniform temperature state may require more time for thermal equilibration than can be achieved in a standard shock wave experiment. Perhaps a starting material of cold pressed submicron sized mineral powder would force a more homogeneous yield process, and hence, more uniform energy dissipation. An accelerated thermal equilibration time should result in this case.

It is interesting to note that the release wave velocities in both corundum (Bless and Ahrens, 1976) and in periclase (present work, Fig. 12) tend toward the expected value for the longitudinal wave speed at the higher stress levels. This would suggest that thermal equilibrium occurs more rapidly at the higher stress levels. The dramatic decrease in rise time of the deforma-

tion wave with increasing Hugoniot stress in periclase (Fig. 10) and the reduction in the shear band separation with increasing strain rate predicted by the Taylor instability analysis (Eq. 40) suggests that the energy dissipation process is more uniform at higher stress levels. Perhaps, then, at Hugoniot stresses far in excess of the elastic limit, the yield process will be sufficiently uniform to allow thermal equilibration within the required time period.

The experimental observations and analysis presented in the present paper point out the importance of technique and the complexity in the shock deformation of certain silicates and oxides. It appears that the dominant compressional features of shock-loaded minerals is strongly influenced by dynamic yielding. A model of heterogeneous yielding to describe the resulting adiabatic shear provides a plausible picture of the resulting shock compression behavior and indicates that material response under shock loading must be considerably more complex than has heretofore been viewed. Because of the importance of quartz, corundum, periclase, and certain other minerals to our understanding of mantle materials, it seems important to proceed with further work to develop a more detailed picture of the shock compression of these materials.

REFERENCES

1. Ahrens, T. J. and G. E. Duvall, "Stress Relaxation Behind Elastic Shock Waves in Rocks," J. Geophys. Res., 71, 4349-4360, 1966.

2. Ahrens, T. J., "High-Pressure Electrical Behavior and Equation of State of Magnesium Oxide from Shock Wave Measurements," J. Appl. Phys., 37, 2532-2541, 1966.

3. Ahrens, T. J., C. F. Petersen, and J. T. Rosenberg, "Shock Compression of Feldspars," J. Geophys. Res., 74, 2727-2746, 1969.

4. Ahrens, T. J., W. H. Gust, and E. B. Royce, "Material Strength Effect in the Shock Compression of Alumina," J. Appl. Phys., 39, 4610-4616, 1968.

5. Ahrens, T. J., and J. T. Rosenberg, Shock Metamorphism: Experiments on Quartz and Plagioclase, in Shock Metamorphism of Natural Materials, B. French and N. Short (eds.) pp. 59-81, Mono Press, Baltimore, Maryland, 1968.

6. Al'tshuler, L. V., S. V. Kormer, M. L. Brazhnik, L. A. Vladimirov, and M. P. Speranskaya, "The Isentropic Compressibility of Aluminum, Copper, Lead, and Iron at High Pressures," Sov. Phys. JETP, 11, 766-775, 1960.

7. Al'tshuler, L. V., M. N. Pavlovskii, and V. P. Drakin, "Peculiarities of Phase Transitions in Compression and Rarefaction Shock Waves," Soviet Phys. JETP, 25, 260-265, 1965.

8. Anan'in, A. V., O. N. Brevsov, A. N. Dremin, S. V. Pershin, and V. F. Tatsii, "The Effect of Shock Waves on Silicon Dioxide. I. Quartz, Combustion, Explosion, and Shock Waves," 10, 426-436, 1974.

9. Andrews, D. J., "Equation of State of the Alpha and Epsilon Phases of Iron," J. Phys. Chem. Solids, 34, 825-840, 1973.

10. Asay, J. R., G. R. Fowles, G. E. Duvall, M. H. Miles, and R. F. Tinder, "Effects of Point Defects on Elastic Decay in LiF," J. Appl. Phys., 43, 2132-2145, 1972.

11. Asay, J. R. and D. B. Hayes, "Shock-Compression and Release Behavior Near Melt States in Aluminum," J. Appl. Phys., 46, 4789-4800, 1975.

12. Barker, L. M., C. D. Lundergan and W. Herrmann, "Dynamic Response of Aluminum," J. Appl. Phys., 35, 1203-1212, 1964.

13. Barker, L. M. and R. E. Hollenbach, "Interferometer Technique for Measuring the Dynamic Mechanical Properties of Materials," Rev. Sci. Inst., 36, 1617, 1965.

14. Barker, L. M., Fine Structure of Compression and Release Wave Shapes in Aluminum Measured by the Velocity Interferometer Technique, in Behavior of Dense Media Under High Dynamic Pressures, Gordon and Breach, New York, 483, 1968.

15. Barker, L. M. and R. E. Hollenbach, "Shock-Wave Studies of PMMA, Fused Silica, and Sapphire," J. Appl. Phys., 41, 4208-4226, 1970.

16. Barker, L. M. and R. E. Hollenbach, "Laser Interferometer for Measuring High Velocities of any Reflecting Surface," J. Appl. Phys., 43, 4669-4675, 1972.

17. Barker, L. M. and K. W. Schuler, "Correction to the Velocity-per-Fringe Relationship for the VISAR Interferometer," J. Appl. Phys., 45, 3692-3693, 1974.

18. Bellman, R. and R. H. Pennington, "Effects of Surface Tension and Viscosity on Taylor Instabilities," Quarterly Appl. Math., 12, 151-162, 1955.

19. Bernstein, D. and D. D. Keough, "Piezoresistivity of Manganin," J. Appl. Phys., 35, 1471-1474, 1964.

20. Bless, S. J. and T. J. Ahrens, "Measurement of Release Wave Speed in Shock-Compressed Polycrystalline Alumina and Aluminum," 11, 1935-1942, 1976.

21. Bogdanov, A. G., S. A. Popov, and V. S. Rudenko, "Location of the Melting Curve of Quartz on the p,T-Diagram of S_iO_2," Translation in Acad. Sci. USSR, Proc. Chem. Section, 201, 1011-1013, 1971.

22. Borg, I. Y., Some Shock Effects in Granodiorite to 270 kbar at the Pile-driver Site, In Flow and Fracture of Rock, H. Heard, I. Borg, N. Carter, and C. Raleigh (eds.) Amer. Geophys. Union, Monograph, 1974.

23. Bridgeman, P. W., "The High Pressure Behavior of Miscellaneous Minerals," Amer. J. Sci., 237, 7-18, 1939.

24. Bridgeman, P. W., "Physics Above 20,000 kg/cm^2," Proc. Roy. Soc. London, A203, 1-17, 1950.

25. Buerger, M. J., "Phase Transformations," Sov. Phys. Crystallography, 16, 959-968, 1972.

26. Bunch, T. E., Some Characteristics of Selected Minerals from Craters, in Shock Metamorphism of Natural Materials, edited by B. French and N. Short, Mono, Baltimore, Md., 1968.

27. Burke, J., The Kinetics of Phase Transformations in Metals, Pergamon Press, 1965.

28. Chao, E. C. T., Pressure and Temperature Histories of Impact Metamorphosed Rocks - Based on petrographic observations, in Shock Metamorphism of Natural Materials, edited by B. French and N. Short, p. 149, Mono, Baltimore, Md., 1968

29. Cowperthwaite, M. and R. F. Willimas, "Determination of Constitutive Relations with Multiple Gauges in Non-divergent Flow," J. Appl. Phys., 42, 456, 1971.

30. DeCarli, P. S. and D. J. Milton, "Stishovite: Synthesis by Shock Wave," Science, 147, 144-145, 1965.

31. DeCarli, P. S., Observations of the Effects of Explosive Shock on Crystalline Solids, in Shock Metamorphism of Natural Materials, edited by B. M. French and N. M. Short, p. 129, Mono, Baltimore, Md., 1968.

32. DeCarli, P. S., "Lagrangian Stress Gauge Study of the Loading and Unloading Response of Raymond Granite," Trans. Am. Geophys. Union, 56, 1061, 1975.

33. Dick, J. J. and D. L. Styris, "Electrical Resistivity of Silver Foils Under Uniaxial Shock-Wave Compression," J. Appl. Phys., 46, 1602-1617, 1975.

34. Dremin, A. N. and G. A. Adadurov, "The Behavior of Glass Under Dynamic Loading," Soviet Phys. Solid State, 6, 1379-1384, 1964.

35. Dremin, A. N., S. V. Pershin, and V. F. Pogorelov, "Structure of Shock Waves in kCℓ and kBr Under Dynamic Compression to 200,000 atm., Combustion, Explosion, and Shock Waves," 1, 1-4, 1965.

36. Dremin, A. N. and O. N. Breusov, "Processes Occurring in Solids Under the Action of Powerful Shock Waves," Russian Chem. Rev. 37, 396-402, 1968.

37. Dremin, A. N. and G. I. Kanel', "Pressure Dependence and Electrical Resistance of Shock-Compressed $C_uN_iM_u$ 3-12 Manganin and $C_uN_iM_u$ 40-1.5 Constantan, Combustion, Explosion and Shock Waves, 8:1, 147-149, 1972.

38. Duvall, G. E. and G. R. Fowles, Shock Waves, in High Pressure Physics and Chemistry II, Academic Press Inc. - London and New York, 1963.

39. Duvall, G. E. and Y. Horic, Shock-induced Phase Transitions, in Proceedings of the Fourth Symposium on Detonation, U.S. Naval Ordnance Laboratory, White Oaks, Maryland, 248-257, 1965.

40. Eden, G. and P. W. Wright, A Technique for the Precise Measurement of the Motion of a Plane Free Surface, in Proceedings of the Fourth International Symposium on Detonation, edited by S. J. Jacobs (Washington, D.C.) 573, 1966.

41. Engelhardt, W. von. and D. Stöffler, Stages of Shock Metamorphism in Crystalline Rocks in the Ries Basin, Germany, in Shock Metamorphism of Natural Materials, B. French and N. Short (eds.) pp. 159-169, Mono Press, Baltimore, Md., 1968.

42. Fowles, G. R., "Dynamic Compression of Quartz," J. Geophys. Res., 72, 5729-5742, 1967.

43. Fowles, G. R. and R. F. Williams, "Plane Stress Wave Propagation in Solids," J. Appl. Phys., 41, 460, 1970.

44. Fowles, G. R., Experimental Technique and Instrumentation, in Dynamic Response of Materials to Intense Impulsive Loading, edited by P. C. Chen and A. K. Hopkins, Air Force Materials Lab, Wright-Patterson AFB, Ohio, 405-480, 1972.

45. Fuller, P. J. A. and J. H. Price, "Dynamic Pressure Measurements to 300 Kilobars with a Resistance Transducer," Brit. J. Appl. Phys., 15, 751-758, 1964.

46. Ginsberg, M. J., D. E. Grady, P. S. DeCarli and J. T. Rosenberg, "Effects of Stress on the Electrical Resistance of Ytterbium and Calibration of Ytterbium Stress Transducers," Stanford Research Institute final rept., Menlo Park, Calif., 1973.

47. Grady, D. E., unpublished, 1970.

48. Grady, D. E., "Experimental Analysis of Attenuating Wave Propagation," Stanford Research Institute Rept. 002-72, Menlo Park, Calif., 1972.

49. Grady, D. E., "Experimental Analysis of Spherical Wave Propagation," J. Geophys. Res., 78, 1299, 1973.

50. Grady, D. E., W. J. Murri, and G. R. Fowles, "Quartz to Stishovite: Wave Propagation in the Mixed Phase Region," J. Geophys. Res., 79, 332-338, 1974.

51. Grady, D. E., W. J. Murri, and P. DeCarli, "Hugoniot Sound Velocities in Two Silicates," Trans. Am. Geophys. Union, 55, 417, 1974.

52. Grady, D. E., W. J. Murri, and P. DeCarli, "Hugoniot Sound Velocities and Phase Transformations in Two Silicates," J. Geophys. Res., 80, 4857-4861, 1975.

53. Grady, D. E., unpublished manuscript, 1976.

54. Grady, D. E., R. E. Hollenbach, K. W. Schuler, and J. F. Callender, "Strain Rate Dependence in Dolomite Inferred from Impact and Static Compression Studies," submitted for publication in J. Geophys. Res., 1976.

55. Graham, R. A., F. W. Neilson, and W. B. Benedick, "Piezoelectric Current from Shock-Loaded Quartz - A Submicrosecond Stress Gauge," J. Appl. Phys., 36, 1775-1783, 1965.

56. Graham, R. A. and W. P. Brooks, "Shock-Wave Compression of Sapphire From 15 to 420 kbar. The Effects of Large Anisotropic Compression," J. Phys. Chem. Solids, 32, 2311-2330, 1971.

57. Graham, R. A. and R. D. Jacobson, "Lithium Niobate Stress Gauge for Pulsed Radiation Deposition Studies," Appl. Phys. Lett., 23, 584-586, 1973.

58. Graham, R. A., "Shock-Wave Compression of X-cut Quartz as Determined by Electrical Response Measurements," J. Phys. Chem. Solids, 35, 355-372, 1974.

59. Graham, R. A. and J. R. Asay, "Measurement of Wave Profiles in Shock-Loaded Solids," to be published in Appl. Mech. Rev., 1976.

60. Gupta, Y. M., G. E. Duvall, and G. R. Fowles, "Dislocation Mechanisms for Stress Relaxation in Shocked LiF," J. Appl. Phys., 46, 532-546, 1975.

61. Gust, W. H. and E. B. Royce, "Dynamic Yield Strengths of Light Armor Materials," Lawrence Livermore Laboratory Rept. UCRL-50901, Livermore, Calif., 1970.

62. Hayes, D. B., "Polymorphic Phase Transformation Rates in Shock-Loaded Potassium Chloride," J. Appl. Phys., 45, 1208-1217, 1974.

63. Herrmann, W., "On the Evaluation of Constitutive Equations from Experiment," Proceedings of the Meeting of the Society of Engineering Science, November 1973.

64. Holtzman, A. H. and G. R. Cowan, The Strengthening of Austenitic Manganese Steel by Plane Shock Waves, in Response of Metals to High Velocity Deformation, Interscience Publishers, New York, 1961.

65. Ingram, G. E. and R. A. Graham, Quartz Gauge Technique for Impact Experiments, in Proceedings of the Fifth Symposium on Detonation, Office of Naval Research, ACR-184, Washington, D.C., 369-386, 1970.

66. Ivanov, A. G. and S. A. Novikov, "Capacitive Data Transmitter for Recording the Instantaneous Velocity of Moving Surfaces," Prib. Tekn. Eksp., 1, 135-139, 1963.

67. Keeler, R. N. and E. B. Royce, Shock Waves in Condensed Media, in Physics of High Energy Density, Academic Press Inc., New York, 51-150, 1971.

68. Keough, D. D., R. F. Williams, and D. Bernstein, in Symposium on High Pressure Technology, (eds. Lloyd and Giardini) American Society of Mechanical Engineers, United Engineering Center, New York, 1964.

69. Keough, D. D., "Procedure for Fabrication and Operation of Manganin Shock Pressure Gauges," Stanford Research Institute Final Rept., Menlo Park, California, 1968.

70. Keough, D. D. and J. I. Wong, "Variation of the Shock Piezo-Resistance Coefficient of Manganin as a Function of Deformation," J. Appl. Phys., 41, 3508-3515, 1970.

71. Klein, M. J., "The Structure of Explosively Shocked MgO Crystals," Phil. Mag., 12, 735-739, 1965.

72. Lyle, J. W., R. L. Shriver, and A. R. McMillan, "Dynamic Piezo-Resistive Coefficient of Manganin to 392 kbar," J. Appl. Phys., 46, 4663-4664, 1969.

73. McQueen, R. G., S. P. Marsh, and J. N. Fritz, "Hugoniot Equation of State of Twelve Rocks," J. Geophys. Res., 72, 4999-5036, 1967.

74. Merrill, L. and W. A. Bassett, "The Crystal Structure of $CaCO^3$ (II), a High-Pressure Metastable Phase of Calcium Carbonate," Acta Crystallogr. B (Denmark), B31, 343-349, 1975.

75. Minshall, S., "Properties of Elastic and Plastic Waves Determined by Pin Contractors and Crystals," J. Appl. Phys., 26, 463-469, 1955.

76. Murri, W. J., D. E. Grady, and K. D. Mahrer, "Equation of State of Rocks," Stanford Research Institute Final Rept., Menlo Park, Calif., 1975.

77. Nunziato, J. C., E. K. Walsh, K. W. Schuler, and L. M. Barker, "Wave Propagation in Nonlinear Viscoelastic Solids," in Handbuch der Physik, Vol. VI a/4 (Cl Truesdell, ed.) Springer-Verlag, 1974.

78. Petersen, C. F., W. J. Murri, and M. Cowperthwaite, "Hugoniot and Release-Adiabat Measurements for Selected Geological Materials," J. Geophys. Res., 75, 2063-2072, 1970.

79. Rice, M. H., "Capacitor Technique for Measuring the Velocity of a Plane Conducting Surface," Rev. Sci. Instr. 32, 449-451, 1961.

80. Ringwood, A. E., A. F. Reid, and A. D. Wadsley, "High-Pressure $KAlSi_3O_8$, An Aluminosilicate with Six-fold Coordination," Acta Crystallogr., 23, 1093-1095, 1967.

81. Schuler, K. W. and D. E. Grady, "Compression Wave Studies in Solenhofen Limestone," Sandia Laboratories Rept., Albuquerque, New Mexico, 1976.

82. Seaman, L., "Lagrangian Analysis for Multiple Stress or Velocity Gauges," J. Appl. Phys., 45, 4303, 1974.

83. Shaner, J. W. and E. B. Royce, "Shock-Induced Demagnetization of YIG," J. Appl. Phys., 39, 492-493, 1968.

84. Singh, A. K. and G. C. Kennedy, "Compression of Calcite to 40 kbar," J. Geophys. Res., 79, 2615-2622, 1974.

85. Spetzler, H., "Equation of State of Polycrystalline and Single-Crystal MgO to 8 kilobars and 800°K," J. Geophys. Res., 75, 2073-2087, 1970.

86. Stishov, S. M. and S. V. Popova, "New Dense Polymorph Modification of Silica," Geochimiya, 10, 837-839, 1961.

87. Stoffler, D., Deformation and Transformation of Rock-Forming Minerals by Natural and Experimental Shock Processes, Fortschr. Mineral., 49, 50-113, 1972

88. Teller, E., "On the Speed of Reactions at High Pressures," J. Chem. Phys., 36, 901-903, 1962.

89. Tyunyaev, Yu. N. et al., Combustion and Explosion, Nauka, Moscow, p. 591, 1972.

90. Wackerle, J., "Shock-Wave Compression of Quartz," J. Appl. Phys., 33, 922-937, 1962.

91. Walsh, J. M. and R. H. Christian, "Equation of State of Metals from Shock Wave Measurements," Phys. Rev., 97, 1544-1556, 1955.

Figure 1 Quartz gauge typical electrode configuration.

Figure 2 Stress wave profile obtained with quartz gauge on MgO. A step stress wave input was provided by impact of an aluminum flyer (0.41 km/s) on the specimen. The stress wave after 3 mm propagation distance was measured at the MgO-quartz interface. 0.2 μs time marks are shown.

Figure 3 Manganin transducer design showing a typical assembly geometry. Bonding is accomplished with epoxy and the gauge plane is normally 25-50 μm.

Figure 4 Stress wave profile obtained with manganin gauge in MgO. A step stress input wave was provided by impact of an aluminum flyer (0.72 km/s). The stress wave profile was measured at an in-material point approximately 3 mm from the impact interface. 0.2 μs time marks are shown.

Figure 5 Manganin stress wave profiles obtained in quartz rock (Arkansas novaculite). The maximum stress achieved was 25 GPa. After Grady et al. (1974).

Figure 6 Electromagnetic transducer design showing typical assembly geometry. ℓ is the length of the active gauge element. The stress wave direction, magnetic field and active gauge element are mutually orthogonal.

Figure 7 Particle velocity profiles obtained in Oakhall limestone. Peak stress equals 12.4 GPa. First and second waves correspond to arrival of the initial shock wave and free surface relief wave, respectively. After Murri et al., 1975.

Figure 8 System schematic of the diffused surface velocity interferometer. Illustrates optical path to and from test specimen, system optics,

and data collecting photomultiplier tubes. Surface acceleration can be distinguished from deceleration by separation of return beam into S and P polarized light displaced 90° in phase. (After Barker and Hollenbach, 1972)

Figure 9 Interferometer fringe pattern and the resulting particle velocity profile obtained in MgO with diffuse surface velocity interferometry. Maximum stress achieved in MgO was approximately 4.8 GPa. Second laser beam provides impact fiducial.

Figure 10 Particle velocity profiles obtained in [100] oriented MgO after approximately 3.3 mm propagation distance. Essential features are the initial elastic precursor, stress relaxation, the subsequent deformation wave, and indications of elastic-plastic response in the release wave. Peak stresses are 4.8, 8.2 and 11.2 GPa.

Figure 11 Comparison of the experimental Hugoniot for MgO and the hydrostat estimated from ultrasonic data (Spetzler, 1970). Also shown are theoretical release stress-volume paths which indicate substantial recovery of material strength at the Hugoniot state.

Figure 12 Elastic and plastic Hugoniot release wave velocities are compared with single crystal MgO longitudinal and bulk sound speeds extrapolated from ultrasonic data (Spetzler, 1970).

Figure 13 (a) Temperature profiles at increasing time due to thermal diffusion from the plane h = 0. (b) Shows a path of constant temperature T_A and the region of material transformed due to temperatures in excess of this value.

Figure 14 Particle velocity profile and the resulting stress-volume path obtained on polycrystalline calcite (Vermont marble). The single crystal calcite hydrostat is also shown (Singh and Kennedy, 1974). The numbered points coordinate various features in the wave profile with corresponding points in the stress-volume curve.

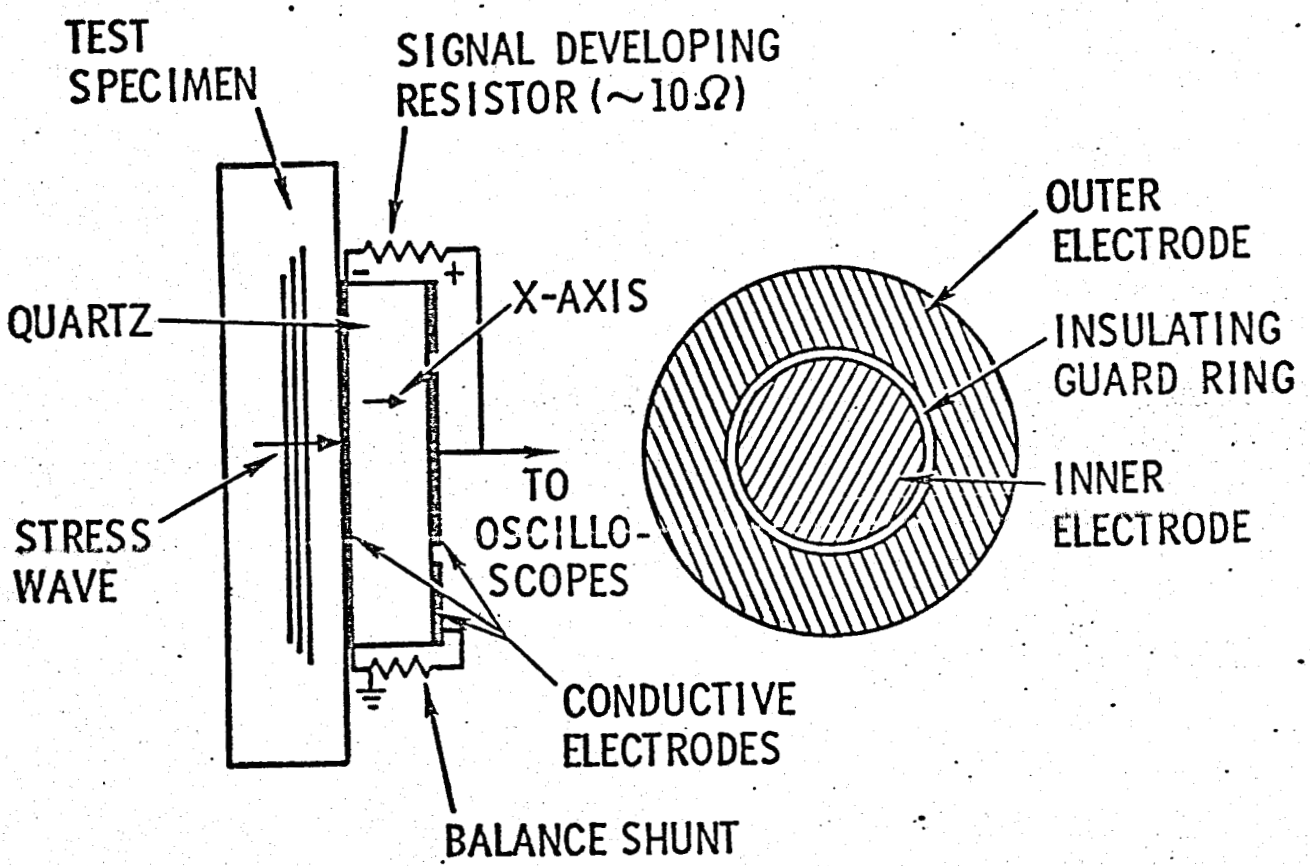
TEST SPECIMEN
SIGNAL DEVELOPING RESISTOR (~10Ω)
OUTER ELECTRODE
QUARTZ
X-AXIS
INSULATING GUARD RING
TO OSCILLO-SCOPES
INNER ELECTRODE
STRESS WAVE
CONDUCTIVE ELECTRODES
BALANCE SHUNT

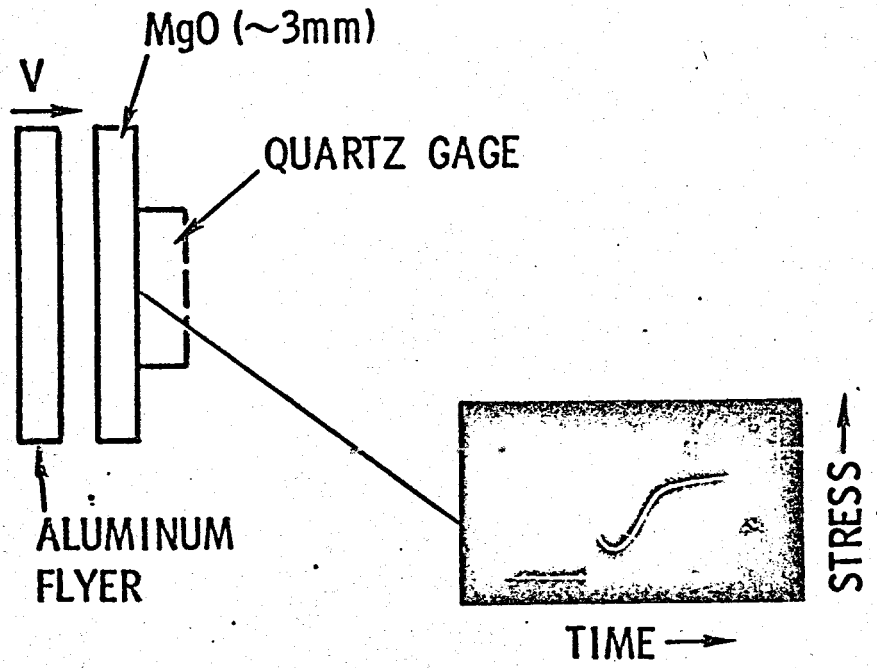
MgO (~3mm)
V
QUARTZ GAGE
ALUMINUM
FLYER
STRESS
TIME

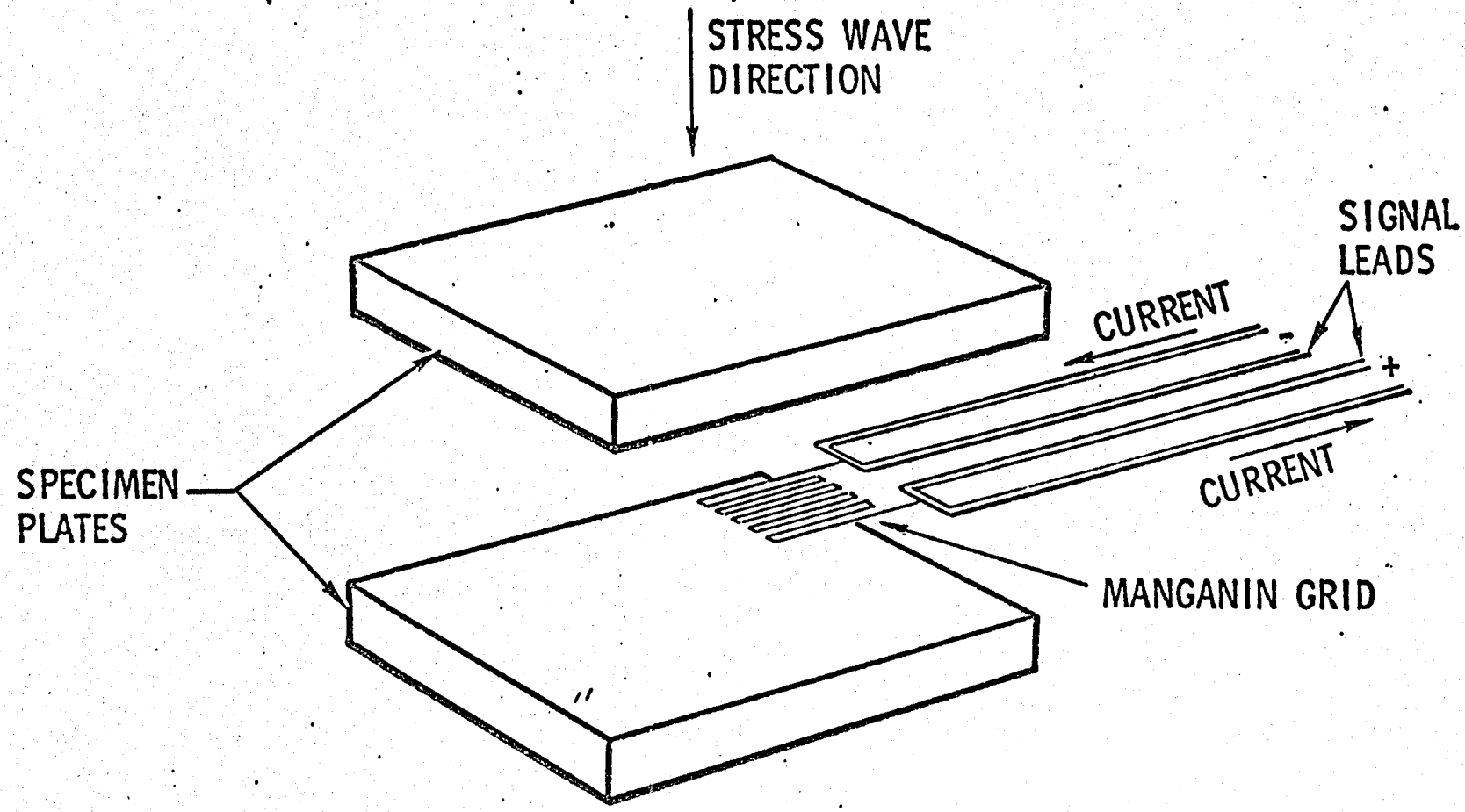
STRESS WAVE
DIRECTION
SIGNAL
LEADS
CURRENT
-
+
CURRENT
SPECIMEN
PLATES
MANGANIN GRID

FIG. 3

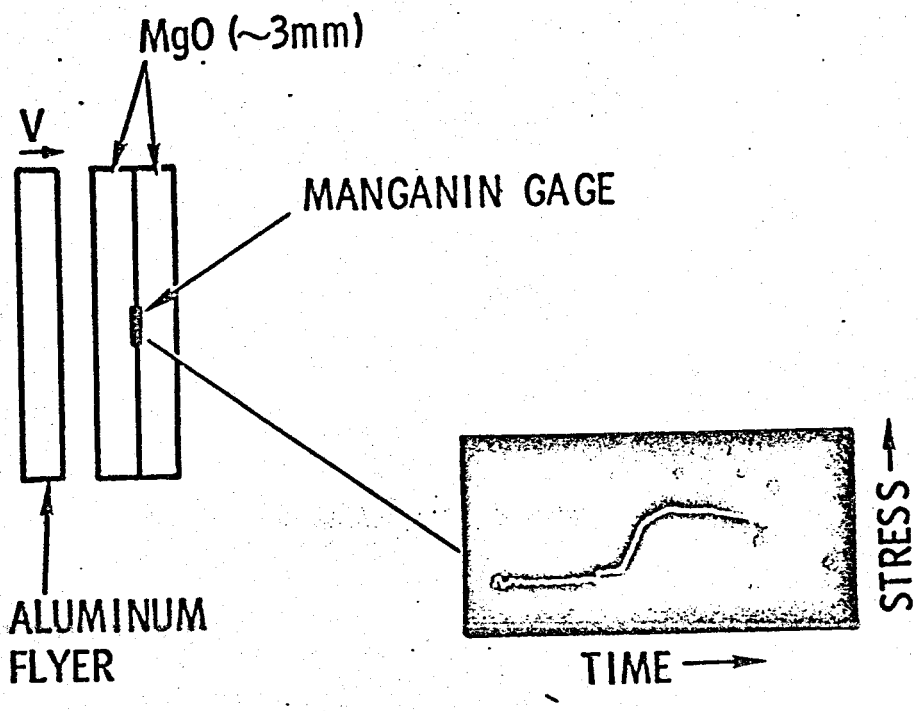
MgO (~3mm)
V
MANGANIN GAGE
ALUMINUM
FLYER
STRESS
TIME

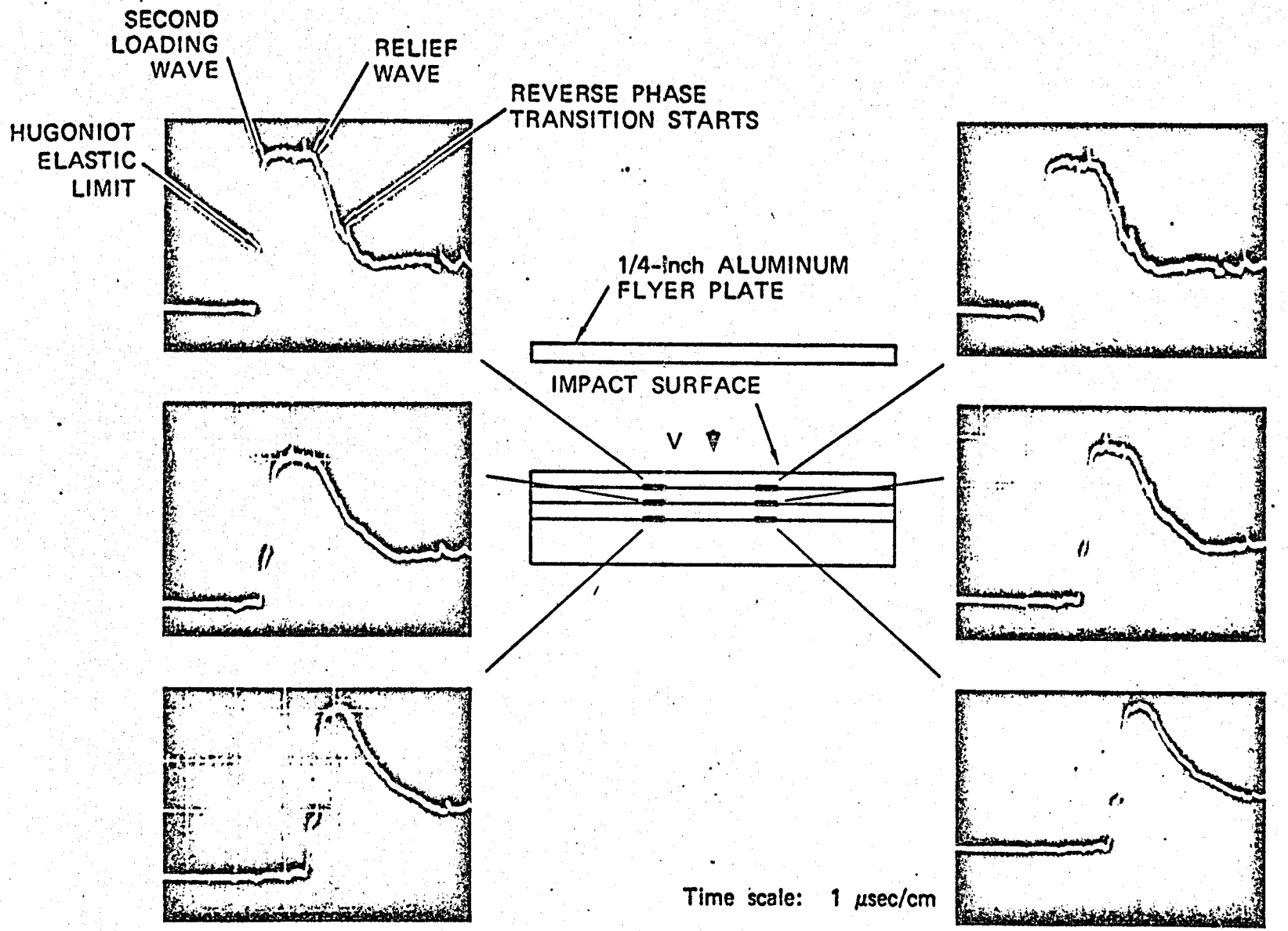
SECOND LOADING WAVE
RELIEF WAVE
REVERSE PHASE TRANSITION STARTS
HUGONIOT ELASTIC LIMIT
1/4-inch ALUMINUM FLYER PLATE
IMPACT SURFACE
V
Time scale: 1 μsec/cm

MA-1883-2B

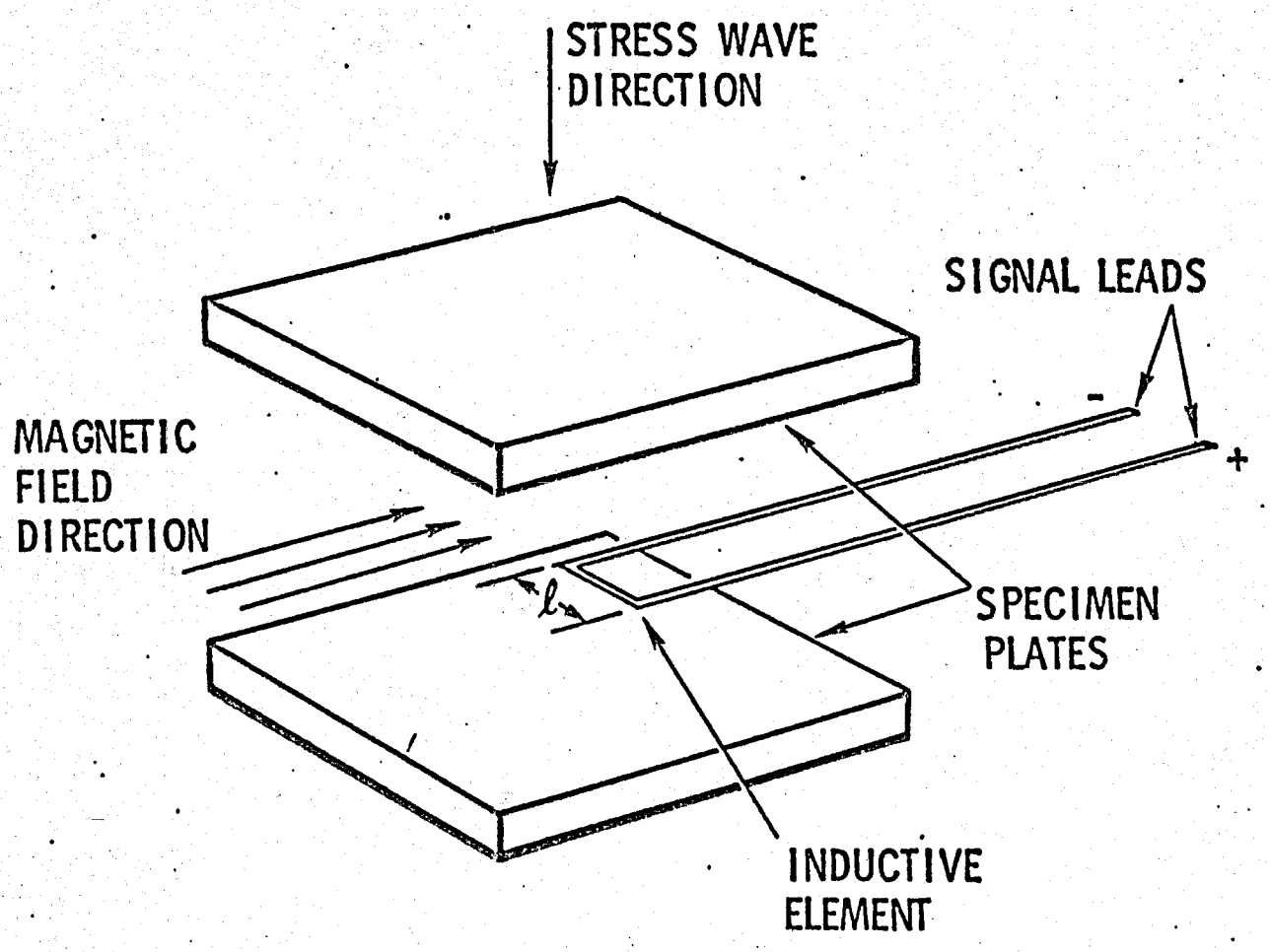
STRESS WAVE
DIRECTION
SIGNAL LEADS
-
+
MAGNETIC
FIELD
DIRECTION
ℓ
SPECIMEN
PLATES
INDUCTIVE
ELEMENT

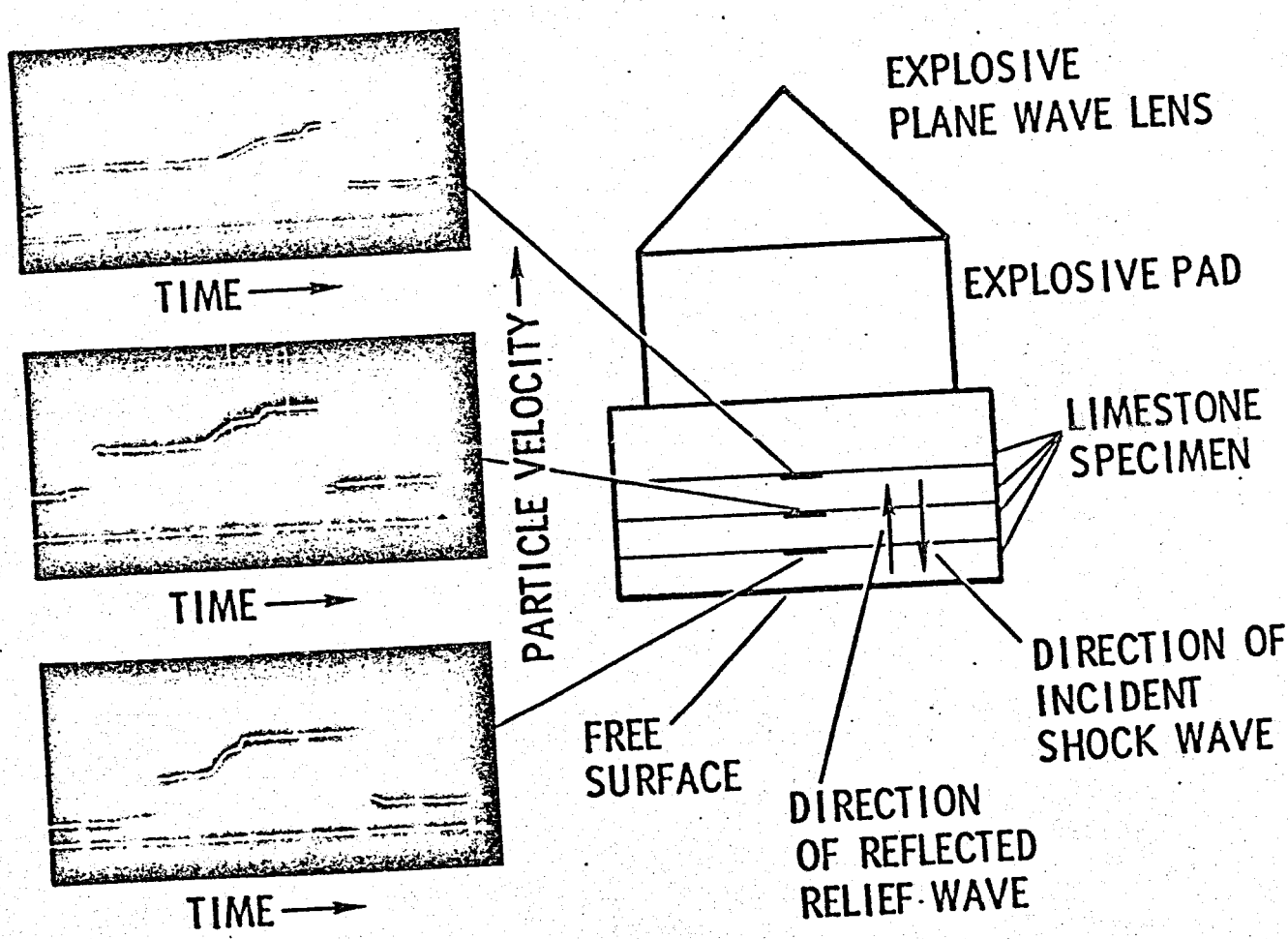
EXPLOSIVE
PLANE WAVE LENS
EXPLOSIVE PAD
LIMESTONE
SPECIMEN
TIME
TIME
TIME
PARTICLE VELOCITY
FREE
SURFACE
DIRECTION
OF REFLECTED
RELIEF WAVE
DIRECTION OF
INCIDENT
SHOCK WAVE

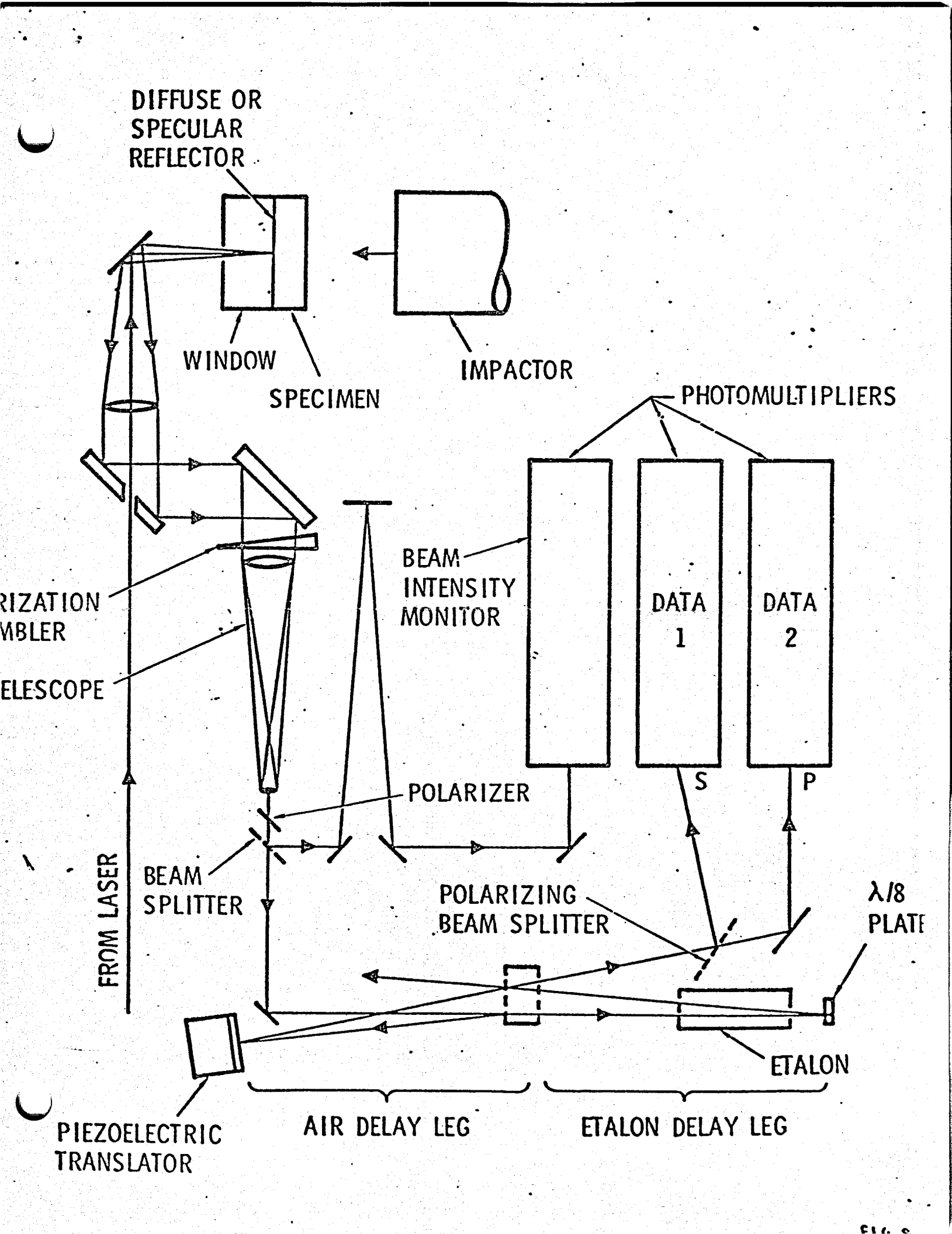
DIFFUSE OR
SPECULAR
REFLECTOR
WINDOW
SPECIMEN
IMPACTOR
PHOTOMULTIPLIERS
RIZATION
MBLER
ELESCOPE
BEAM
INTENSITY
MONITOR
DATA
1
DATA
2
S
P
POLARIZER
FROM LASER
BEAM
SPLITTER
POLARIZING
BEAM SPLITTER
λ/8
PLATE
ETALON
PIEZOELECTRIC
TRANSLATOR
AIR DELAY LEG
ETALON DELAY LEG

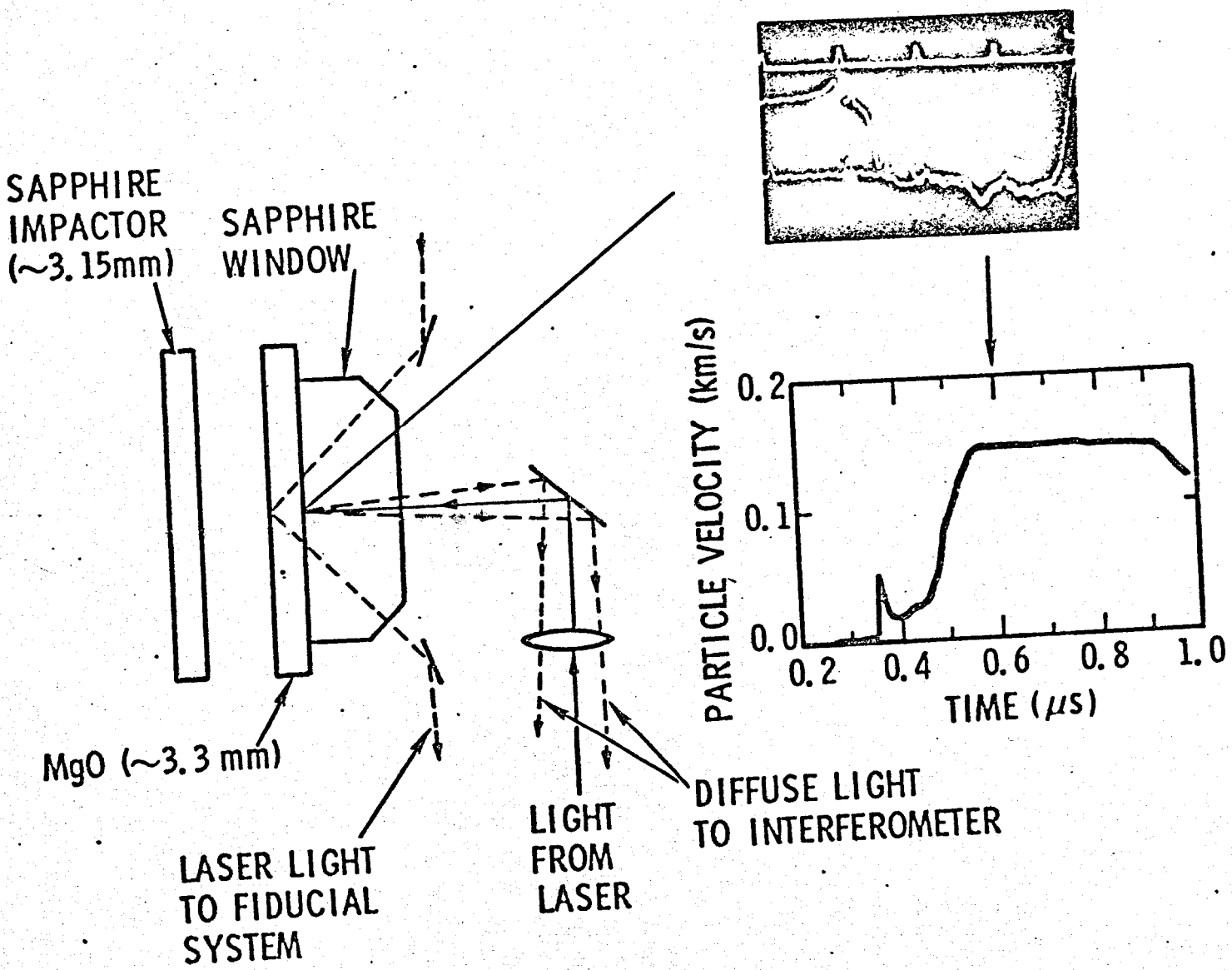
SAPPHIRE IMPACTOR (~3.15mm)
SAPPHIRE WINDOW
MgO (~3.3 mm)
LASER LIGHT TO FIDUCIAL SYSTEM
LIGHT FROM LASER
DIFFUSE LIGHT TO INTERFEROMETER
PARTICLE VELOCITY (km/s)
0.2
0.1
0.0
0.2
0.4
0.6
0.8
1.0
TIME (μs)

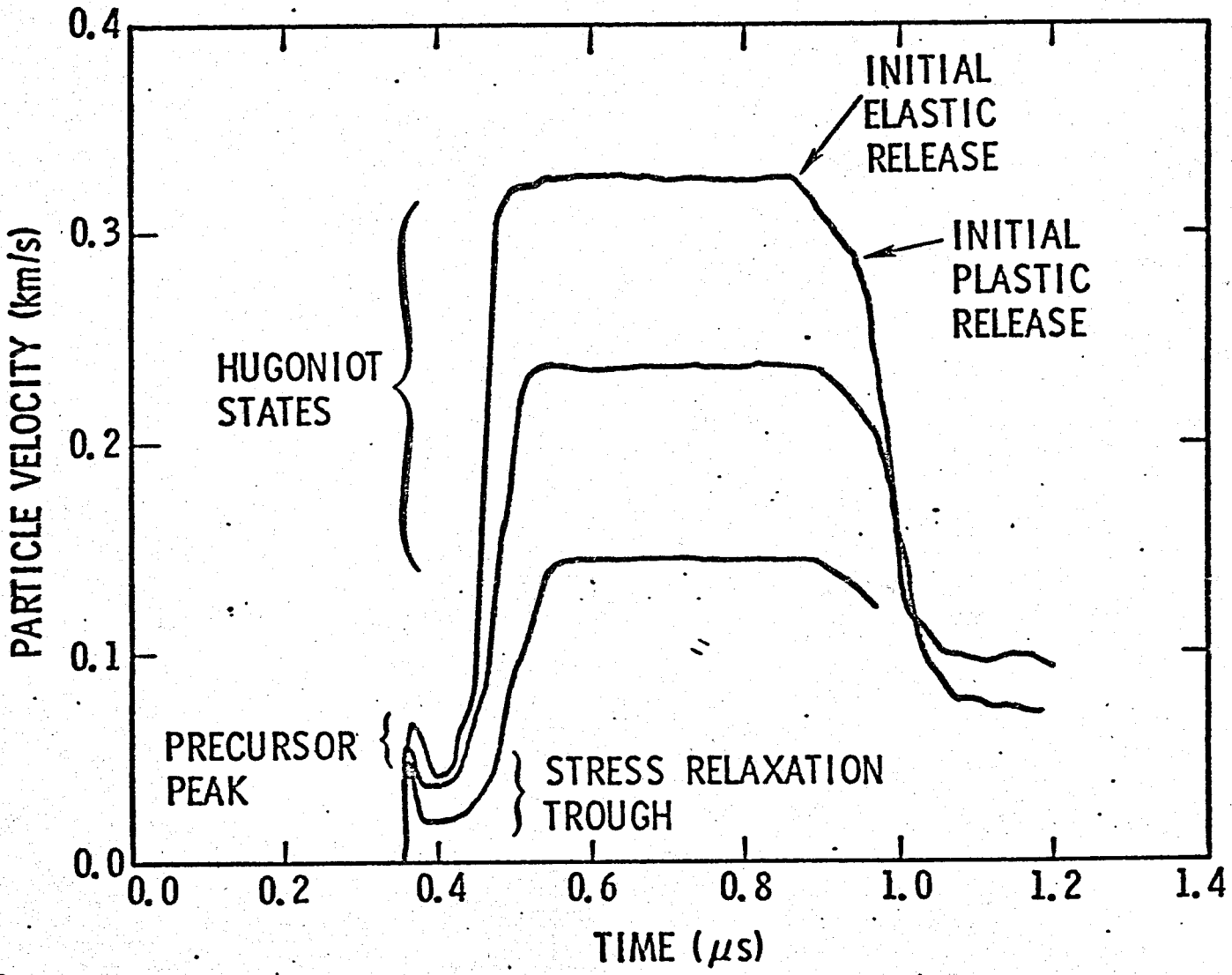
0.4
0.3
0.2
0.1
0.0
PARTICLE VELOCITY (km/s)
INITIAL
ELASTIC
RELEASE
INITIAL
PLASTIC
RELEASE
HUGONIOT
STATES
PRECURSOR
PEAK
STRESS RELAXATION
TROUGH
0.0
0.2
0.4
0.6
0.8
1.0
1.2
1.4
TIME (μs)

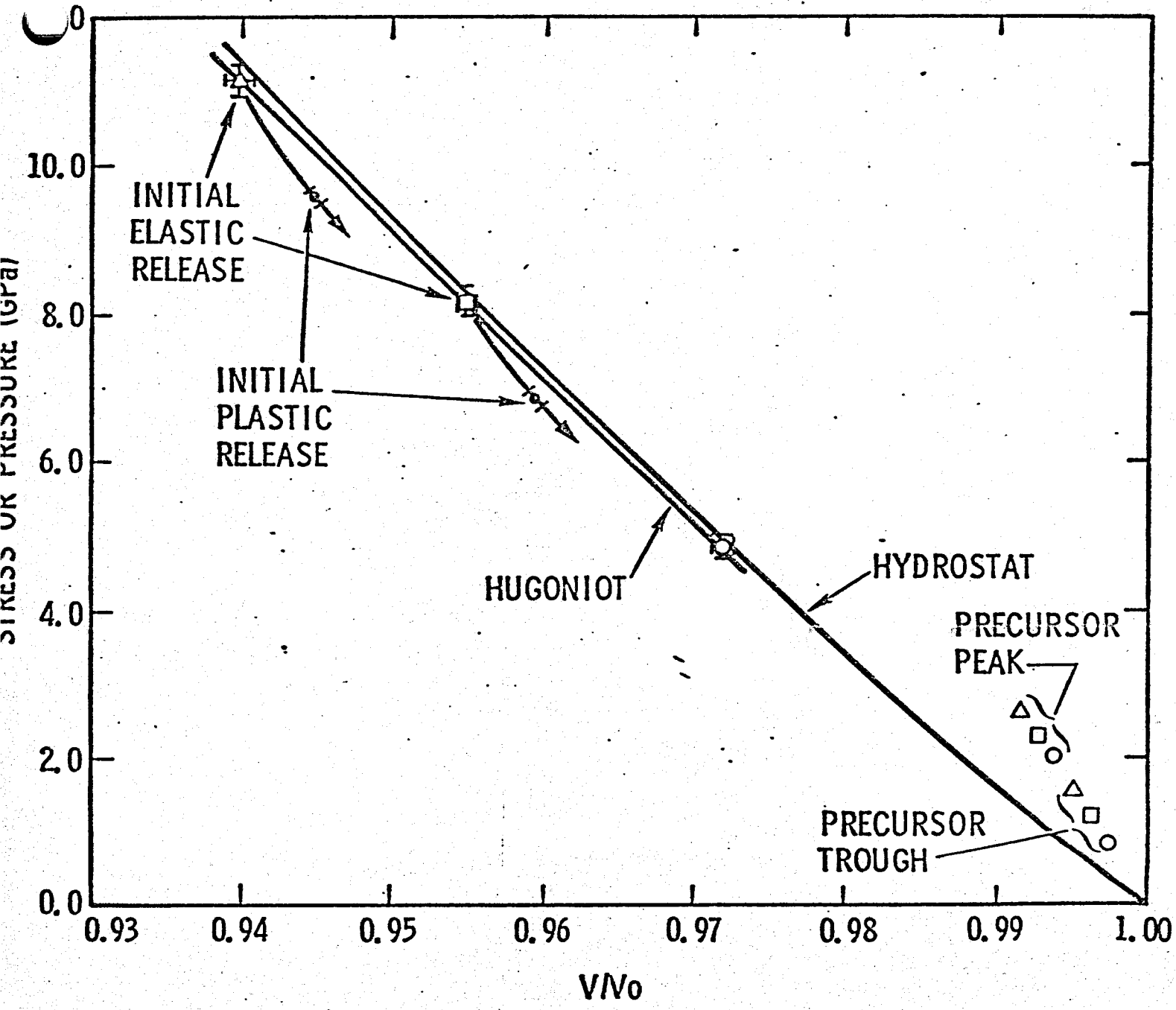
STRESS OR PRESSURE (GPa)
0
10.0
8.0
6.0
4.0
2.0
0.0
INITIAL
ELASTIC
RELEASE
INITIAL
PLASTIC
RELEASE
HUGONIOT
HYDROSTAT
PRECURSOR
PEAK
PRECURSOR
TROUGH
0.93
0.94
0.95
0.96
0.97
0.98
0.99
1.00
V/Vo

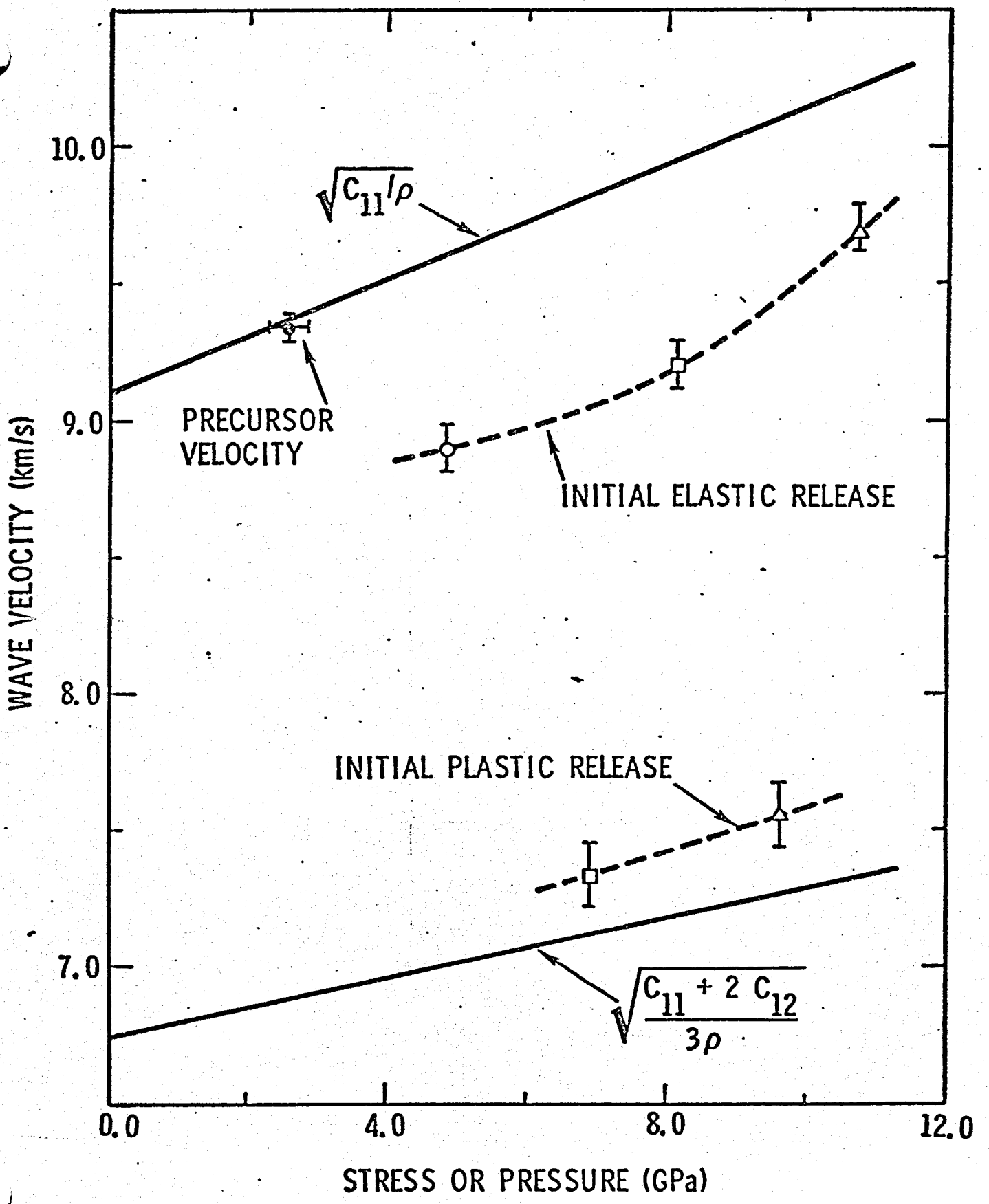
10.0
9.0
8.0
7.0
WAVE VELOCITY (km/s)
$\sqrt{C_{11}/\rho}$
PRECURSOR VELOCITY
INITIAL ELASTIC RELEASE
INITIAL PLASTIC RELEASE
$\sqrt{\frac{C_{11} + 2\,C_{12}}{3\rho}}$
0.0
4.0
8.0
12.0
STRESS OR PRESSURE (GPa)

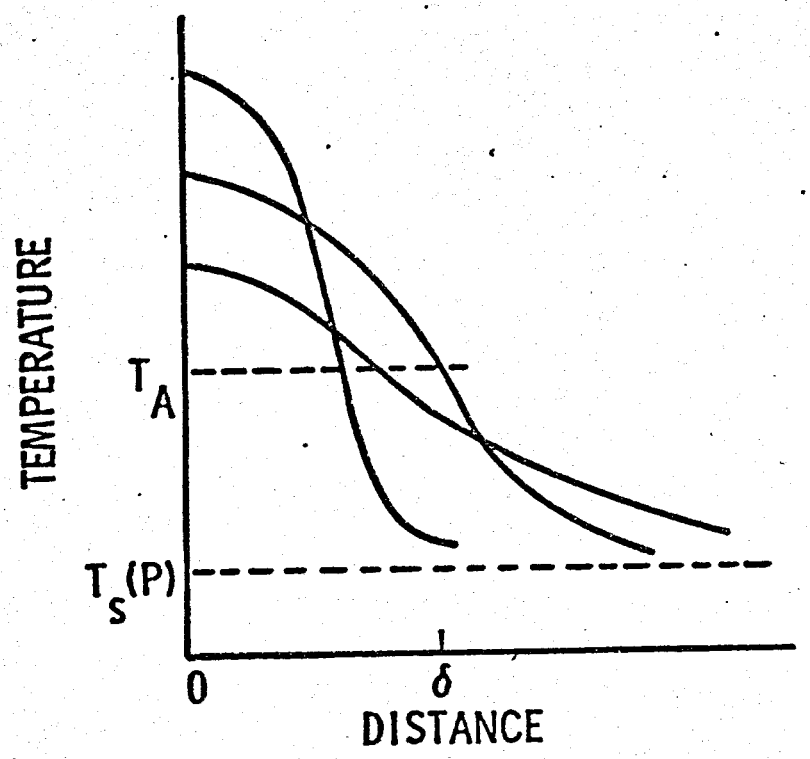
TEMPERATURE
T_A
$T_s(P)$
0
δ
DISTANCE

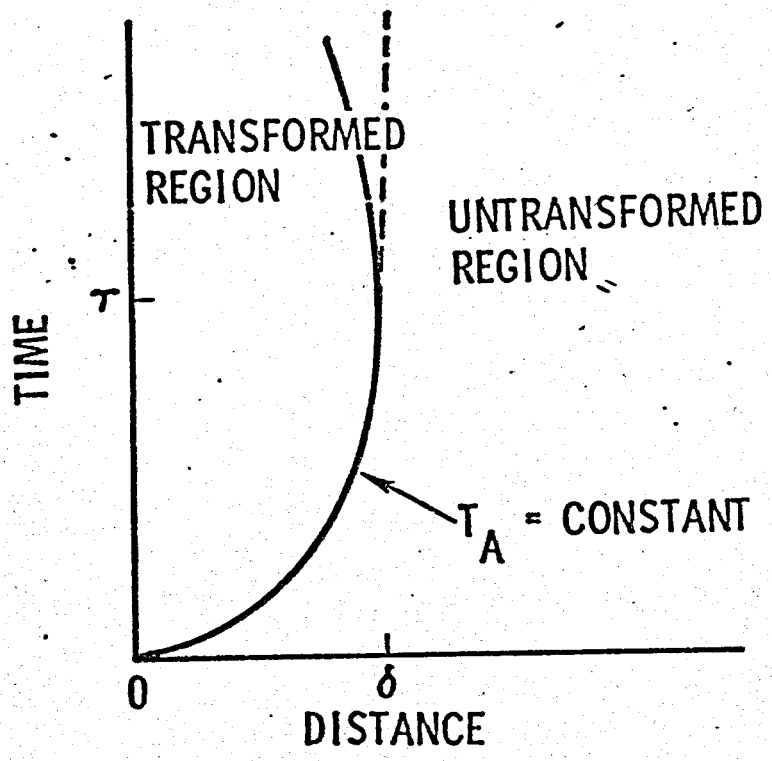
TRANSFORMED REGION
UNTRANSFORMED REGION
TIME
τ
T_A = CONSTANT
0
δ
DISTANCE

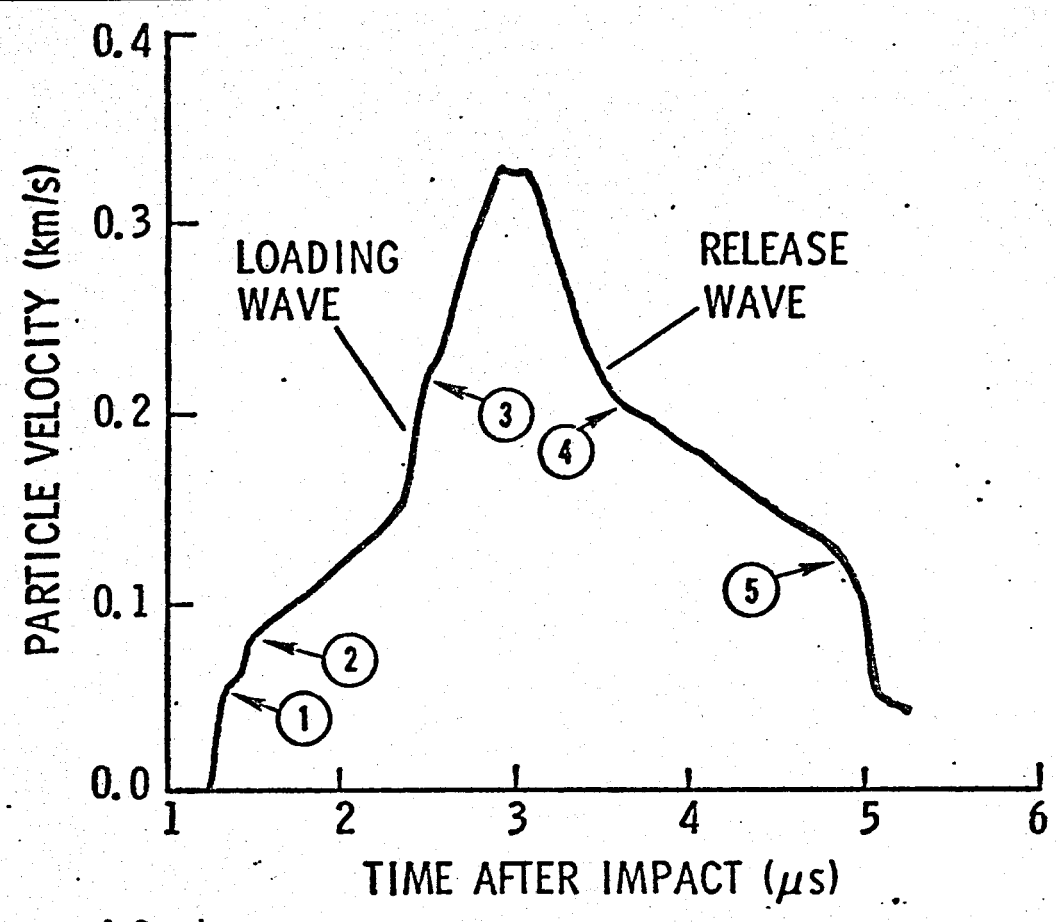
0.4
0.3
0.2
0.1
0.0
PARTICLE VELOCITY (km/s)
LOADING WAVE
RELEASE WAVE
1
2
3
4
5
1
2
3
4
5
6
TIME AFTER IMPACT (μs)

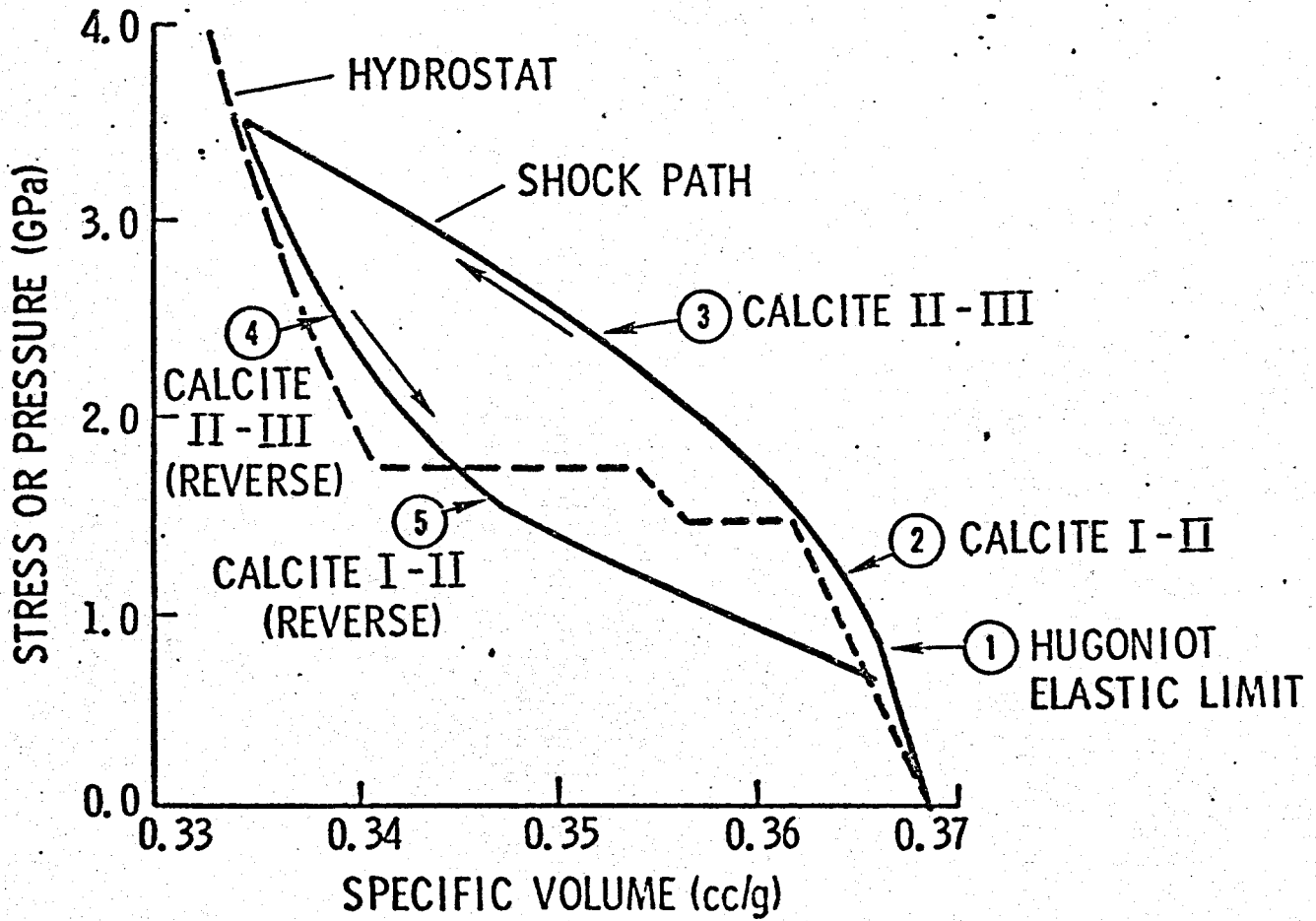
4.0
3.0
2.0
1.0
0.0
STRESS OR PRESSURE (GPa)
HYDROSTAT
SHOCK PATH
3 CALCITE II - III
4
CALCITE II - III (REVERSE)
5
CALCITE I - II (REVERSE)
2 CALCITE I - II
1 HUGONIOT ELASTIC LIMIT
0.33
0.34
0.35
0.36
0.37
SPECIFIC VOLUME (cc/g)

FIG 14